**NATIONAL TECHNICAL UNIVERSITY OF ATHENS**
**Joint Postgraduate Course of Computational Mechanics**

# MASTER THESIS

# ELEFTHERIOS KOUKOULOPOULOS

## Adjoint-Based Optimization of

## Hydrodynamic Lubrication Problems

**Advisors:**

**K. C. Giannakoglou, Professor NTUA,**
   **School of Mechanical Engineering**

**C. Papadopoulos, Assistant Professor NTUA,**
   **School of Naval Architecture and Marine Engineering**

**Athens, September 2016**

# Abstract

In the present thesis, hydrodynamically lubricated contacts are optimized using the continuous adjoint method and a simplified (1D) flow model. Such contacts can be found in almost any mechanical system and they are the main source of friction, which is responsible for power losses, material wear and even total failure of the component. Friction contacts operate under the regime of hydrodynamic lubrication, meaning that a thin fluid film separates the two interacting surfaces, in order to avoid metal to metal contact. So, optimization of the geometry design of sliding surfaces is critical for the reduction of power loss and wear. Optimization is performed aims either the maximization of load capacity or the minimization of the friction coefficient.

For the purposes of optimization, the continuous adjoint-based method has been selected. Adjoint-methods belong to the wider category of deterministic optimization methods, which compute and use the derivative of the objective function. They are mathematical tools for the calculation of the gradient of an objective function, satisfying at the same time the primal equations describing the problem. The equation describing the hydrodynamic lubrication problem will be the Reynolds equation. The main benefit of the adjoint method is that the cost of the computation of the derivatives is almost equal to the cost of numerically solving the primal equation and completely independent of the number of design variables.

So, several different geometries have been studied, representing the hydrodynamic slider found in mechanical components, with the use of the adjoint optimization method, aiming at the maximization of load capacity and for one case the minimization of friction coefficient additionally. For each different geometry case, the amount of design variables varies and the mathematical formulation is different and for that it is explained for each geometry in detail in the sub-chapters of Chapter 4. The chosen slider geometries are: simple converging slider (optimized for both load capacity and friction coefficient), converging and diverging slider and step slider (only load capacity). One last case has also been studied, where the design variables are the film thickness of each discretization point, meaning that their amount is equal to the number of grid points. Ideally with this method the geometry could take any possible shape and self-adjust to each case.

# Εκτενής Περίληψη

Στην μεταπτυχιακή αυτή εργασία πραγματοποιήθηκε βελτιστοποίηση τριβολογικών επιφανειών με τη μέθοδο της συνεχούς συζυγούς μεθόδου. Αυτές οι επιφάνειες συναντιούνται σε πολλά μηχανολογικά συστήματα και κυρίως στις μηχανές Diesel. Σε αυτές αναπτύσσονται δυνάμεις τριβής, οι οποίες ευθύνονται για απώλειες ισχύος, απώλεια υλικού και, τελικά, ακόμη και ολική αστοχία της κατασκευής. Οι ολισθητήρες τριβής λειτουργούν υπό το καθεστώς υδροδυναμικής λίπανσης, με την έννοια ότι ένα λεπτό φιλμ λιπαντικού υγρού διαχωρίζει τις δύο συνεργαζόμενες επιφάνειες, ώστε να αποφεύγεται η μεταξύ τους επαφή. Έτσι η βελτιστοποίηση της γεωμετρίας αυτών των επιφανειών είναι καίρια για τη μείωση των απωλειών ενέργειας και της φθοράς. Η βελτιστοποίηση εκτελείται σκοπεύοντας είτε τη μεγιστοποίηση του αδιάστατου παραλαμβανόμενου φορτίου είτε την ελαχιστοποίηση του αδιάστατου συντελεστή τριβής.

Για την υλοποίηση της διαδικασίας βελτιστοποίησης χρησιμοποιήθηκε η συνεχής συζυγής μέθοδος, η οποία ανήκει στην ευρύτερη κατηγορία των ντετερμινιστικών μεθόδων βελτιστοποίησης και που δουλεύουν με την παράγωγο της αντικειμενικής συνάρτησης. Είναι μαθηματικά εργαλεία για τον υπολογισμό της παραγώγου της αντικειμενικής συνάρτησης, πληρώντας ταυτόχρονα τις εξισώσεις ρευστών που περιγράφουν το φυσικό πρόβλημα. Η εξίσωση που διέπει την υδροδυναμική λίπανση είναι η απλοποιημένη εξίσωση Reynolds. Το σημαντικότερο πλεονέκτημα της συζυγούς μεθόδου είναι ότι το κόστος υπολογισμού των παραγώγων είναι σχεδόν ίσο με το κόστος επίλυσης της εξίσωσης ρευστών και εντελώς ανεξάρτητο από το πλήθος των παραμέτρων σχεδίασης.

Μελετήθηκαν τέσσερις διαφορετικές γεωμετρίες υδροδυναμικών ολισθητήρων στοχεύοντας σε όλες στη μεγιστοποίηση του αδιάστατου παραλαμβανόμενου φορτίου και σε κάποιες στην ελαχιστοποίηση του αδιάστατου συντελεστή τριβής. Οι γεωμετρίες που μελετήθηκαν είναι οι εξής: απλός συγκλίνων ολισθητήρας, συγκλίνων-αποκλίνων ολισθητήρας και ολισθητήρας σε σχήμα σκαλοπατιού. Το τέταρτο σενάριο αφορά πάλι τον απλό ολισθητήρα με διαφορετική παραμετροποίηση, όπου οι μεταβλητές σχεδιασμού είναι ουσιαστικά η τοπική τιμή του ύψους του λιπαντικού φιλμ, που σημαίνει ότι το πλήθος των μεταβλητές σχεδιασμού είναι ίσο με το πλήθος των κόμβων διακριτοποίησης του προβλήματος. Σε όλα τα παραπάνω προβλήματα επιβλήθηκε περιορισμός στην ελάχιστη τιμή του πάχους λιπαντικού, υπό την έννοια ότι η τοπική τιμή του πάχους λιπαντικού δεν πρέπει να γίνεται μικρότερη από μία συγκεκριμένη τιμή. Στην αντίθετη περίπτωση όπου το ελάχιστο πάχος θα ήταν και αυτό μεταβλητές σχεδιασμού , το πρόβλημα της βελτιστοποίησης θα είχε τετριμμένη λύση τη μηδενική.

Στην περίπτωση του απλού κεκλιμένου ολισθητήρα η γεωμετρία του λιπαντικού φιλμ παραμετροποιήθηκε με μία μόνο μεταβλητή σχεδιασμού, αυτή της κλίσης του καναλιού. Χρησιμοποιήθηκε για να γίνει πιστοποίηση των αποτελεσμάτων, όσον αφορά το αδιάστατο παραλαμβανόμενο φορτίο (μεγιστοποίηση) και συντελεστή ολίσθησης (ελαχιστοποίηση), με αναφορές από τη διεθνή βιβλιογραφία και διαπιστώθηκε πολύ καλή ταύτιση. Για το αδιάστατο παραλαμβανόμενο φορτίο η βέλτιστη τιμή του είναι $W^*=0.0267$ και αντιστοιχεί σε κλίση k=1.2, ενώ για τον αδιάστατο συντελεστή τριβής η βέλτιστη τιμή του είναι $f^*=4.5$ και αντιστοιχεί σε τιμή της κλίσης k=1.55 .

Στη δεύτερη περίπτωση, συγκλίνων-αποκλίνων ολισθητήρας, η παραμετροποίηση της γεωμετρίας έγινε με τρεις μεταβλητές σχεδιασμού, τα ύψη εισροής και εκροής του ρευστού και τη διαμήκη θέση αλλαγής της κλίσης. Η βελτιστοποίηση πραγματοποιήθηκε όσον αφορά το αδιάστατο παραλαμβανόμενο φορτίο (μεγιστοποίηση). Ξεκινώντας κάθε φορά από διαφορετικό σημείο διακριτοποίησης, δηλαδή διαφορετικό συνδυασμό των αρχικών τιμών των μεταβλητών σχεδιασμού, η μέθοδος κατέληξε στο ίδιο σημείο W*=0.032055 και για μεταβλητές σχεδίασης $h_1$=120 μm, $h_2$=50 μm και l=0.040073 m . Έτσι μπορούμε να ισχυριστούμε ότι αυτό το σημείο είναι ένα εν δυνάμει ολικό βέλτιστο.

Στην τρίτη περίπτωση του ολισθητήρα με σχήμα σκαλοπάτι, η γεωμετρία αποτυπώθηκε με δύο μεταβλητές σχεδιασμού, το ύψος εισόδου του ρευστού και τη διαμήκη θέση του σκαλοπατιού. Αντικειμενική συνάρτηση που έπρεπε να μεγιστοποιηθεί ήταν το αδιάστατο παραλαμβανόμενο φορτίο. Ομοίως με την προηγούμενη περίπτωση η βελτιστοποίηση ξεκίνησε από τρεις διαφορετικούς συνδυασμούς αρχικών τιμών των μεταβλητών σχεδιασμού και όλοι κατέληξαν στο ίδιο βέλτιστο σημείο με τιμή της αντικειμενικής συνάρτησης W*=0.03423 και τιμές των μεταβλητών σχεδιασμού $h_1$=93 μm και l=0.034055 m . Και σε αυτό το σημείο μπορούμε να ισχυριστούμε ότι η παραπάνω λύση είναι πιθανώς το καθολικό βέλτιστο.

Στην τελευταία περίπτωση, η γεωμετρία είναι αυτή του απλού συγκλίνοντα ολισθητήρα με διαφορετικό όμως τρόπο παραμετροποίησης. Οι μεταβλητές σχεδιασμού είναι οι κομβικές τιμές του ύψους του λιπαντικού φιλμ. Το κίνητρο που μας οδήγησε σε αυτή τη σκέψη, καθώς και το βασικότερο πλεονέκτημα αυτής της παραμετροποίησης, είναι ότι η γεωμετρία είναι ελεύθερη να λάβει οποιοδήποτε δυνατό σχήμα. Ακόμη, εδώ εκμεταλλευόμαστε και το σημαντικότερο πλεονέκτημα της συζυγούς μεθόδου, κατά το οποίο το κόστος υπολογισμού των παραγώγων είναι ανεξάρτητο από το πλήθος των μεταβλητών σχεδιασμού και περίπου ίσο με το κόστος επίλυσης των εξισώσεων του ρευστού του αρχικού προβλήματος. Η μεγαλύτερη δυσκολία σε αυτή την περίπτωση ήταν να αναπτυχθούν οι όροι που υπολογίζουν τις παραγώγους ευαισθησίας, καθώς και να πιστοποιηθούν οι τιμές των παραγώγων αυτών που προκύπτουν από τη συζυγή μέθοδο με τις παραγώγους που προκύπτουν από τις πεπερασμένες διαφορές. Ξεκινώντας πάλι από διαφορετικά αρχικά σχήματα, και κυρίως με διαφορετικές αρχικές κλίσεις, προέκυψε κάθε φορά σε διαφορετικό τελικό αποτέλεσμα, δηλαδή αναλόγως την αρχικοποίηση, εντοπίζοντας διαφορετικό τοπικό βέλτιστο.

Συμπερασματικά, η συνεχής συζυγής μέθοδος είναι ένα πολύ χρήσιμο εργαλείο για τη βελτιστοποίηση τριβολογικών επιφανειών. Ακόμη και αν δεν τερματιστεί η βελτιστοποίηση, με τη μέθοδο αυτή μπορούμε να κατασκευάσουμε έναν χάρτη ευαισθησίας της γεωμετρίας, ο οποίος μας υποδεικνύει ποιες περιοχές της επιφάνειας θα προκαλέσουν μεγαλύτερη αλλαγή στην αντικειμενική συνάρτηση αν μετακινηθούν τα σημεία της, και άρα πού πρέπει να γίνει παρέμβαση προκειμένου να εντοπιστεί η επιθυμητή τιμή της αντικειμενικής συνάρτησης, είτε μέγιστο είτε ελάχιστο.

# Table of Contents

# Nomenclature

| | |
|---|---|
| *Eta* | Steepest descent step factor |
| *F* | Friction force [N] |
| *F* | Friction coefficient, $f = F/W$ |
| $f^*$ | Non-dimensional friction coefficient, $f^* = f \cdot L / h_0$ |
| *H* | Film thickness [m] |
| $h_1$ | Outlet height [m] |
| $h_{min}$, $h_0$ | Minimum film thickness [m] |
| *K* | Converging ratio, $k = (h_1 - h_0)/h_0$ |
| *L* | Slider length [m] |
| *M* | Sigmoidal function magnitude factor |
| *P* | Pressure jj[Pa] |
| *U* | Velosity [m/s] |
| *u* | Fluid velocity in the x direction [m/s] |
| *v* | Fluid velocity in the y direction [m/s] |
| *W* | Load carrying capacity of fluid [N] |
| *w* | Fluid velocity in the z direction [m/s] |
| $W^*$ | Non-dimensional load carrying capacity |
| *x* | Direction along the piston ring profile (streamwise direction) |
| *z* | Direction along the film thickness (crossflow direction) |
| $\mu$ | Lubricant dynamic viscosity [Pa s] |
| $\rho$ | Lubricant density [kg/m$^3$] |
| $\tau$ | Shear stress [Pa] |

# List of Figures

11

# List of Tables

# 1. Introduction

## 1.1 Tribology

Tribology is a rather new field of science, which studies friction, wear and lubrication of mechanical parts. It meets application in a variety of devices, from household appliances to bigger and more complicated structures, such as ships. Tribology of a certain component can be studied under several scopes, such as numerically, experimentally, materials etc. Friction is the major cause of wear, which if not limited it can cause serious material damage and, finally, total failure of the component. Wear may be substantially reduced when a thin layer (film) of material, usually liquid, but also gas or solid, separates the two sliding surfaces. Hydrodynamic lubrication has been a subject of extensive research in recent decades, in order to study the behavior of mechanical components such as bearings, piston rings, seals etc. Consequently, improvements of the geometry design and, even, optimization of them can substantially reduce friction and wear, increasing the lifetime of a component and reducing the operational costs. Such improvements are of utmost importance, knowing that 15-25% of the total energy consumption worldwide is used to overcome friction [1].

Large two stroke marine Diesel engines are a typical case where the study of tribology could contribute to the minimization of energy losses and wear of the interacting surfaces. These engines can be found installed in large over-seas ships, such as crude oil carriers, tankers and containerships. In these engines it is estimated that 5-7% of the total generated power is consumed in mechanical friction [2]. The generated power of a large two stroke engine can surpass the amount of 80000 kW, meaning that friction losses consist a significant loss of energy. More specifically friction in a large two stroke marine engine is distributed in the several individual parts as follows: piston ring pack (26%), guide shoe bearings (31%), main bearings (23%) and the connecting rod bearings (10%), as seen in [3].

The common feature shared between the mechanical components described above is the existence of a wedge-shaped lubricating film and the relative motion of one surface to the other. These two conditions are both necessary for the occurrence of hydrodynamic lubrication, which is the phenomenon due to which the two interacting surfaces are separated. Consequently, optimizing the geometry of the interacting surfaces, in terms of load carrying capacity and friction power, is crucial for reducing friction losses in a Diesel engine. Load capacity must be maximized, because higher values mean that the slider can withstand higher loads for the same lubricant film thickness, while friction power should be minimized, in order to reduce the power consumed for overcoming friction.

## 1.2 Optimization methods (based on [4] and [5])

The process of optimization can be defined as the process of obtaining the "best", provided that there is a way of measuring what is "good" and what is "bad". Practically, in different problems someone aims at the maximum of a quantity (e.g. income) or the least of a quantity (e.g. workforce), meaning that the term optimum can either correspond to the maximum or the minimum, depending on the different circumstances of each problem.

Optimization problems can occur in almost all scientific fields, such as engineering, economics, mathematics, commerce, social sciences, geopolitics etc. As for engineering, some examples of subdomains that optimization is important are: aeronautics, naval architecture, electronics, civil and chemical engineering etc. In these areas, optimization is implemented in order, for example, to find the best design of devices, such as the best set-up of circuits in order to minimize the size of a smartphone, to design an optimal airfoil for minimum drag or even a bridge for the best behavior under extreme weather conditions. So, it is obvious that optimization methods are in widespread use and at the same time very useful in order to improve all the aspects of human life.

Before proceeding, optimization must be formulated in a mathematical way. The most common way to present an optimization problem is by deriving a performance criterion F (objective function) in terms of a number of parameters (design parameters) $x_i$.

$$F = f\left(x_1, x_2, \ldots, x_n\right)$$

Objective function F is a scalar quantity which can assume any possible form, being either a cost of a product or the drag of an airfoil. Design variables $x_i$ are the parameters that determine the value of the objective function F. They can either be independent parameters, such as the weather conditions, which are mostly unpredictable, or control parameters that can be properly adjusted by the designer performing the optimization.

Therefore, the optimization is applied in order to find the combination of the design variables values $xi$ that minimize or maximize the objective function F.

The optimization problems used in engineering applications can be classified as presented below.

### 1.2.1 Continuous - Discrete problems

A basic classification of optimization problems is into continuous and discrete problems. Continuous problems consider real variables as degrees of freedom (design variables), being either constrained within certain bounds or not. It is obvious that, in continuous problems, the optimal solution is being searched within an infinite number of possible solutions. An example of a continuous optimization problem would be the finding of the optimal dampening coefficient of the suspension of a car, in order to minimize the vibrations of the cabin, where the coefficient can take any real value. In discrete optimization problems, the possible solutions are integer numbers or boolean and are included within a finite amount (which could also be very large) of desired solutions. An example of a discrete optimization would be the selection of the number of propeller blades of a ship, in order to maximize the performance factor of the propeller, where the amount of blades can only be an integer number. In most of cases, continuous problems have continuous objective and/or constraint functions that can be differentiated. A common practice to cope with discrete optimization problems is to solve them as continuous and afterwards to round up the result to the closest integer, but this usually yields a result far from the actual optimal solution. The problem of optimization to be solved in this thesis is a continuous one.

### 1.2.2 Deterministic – Stochastic methods

The optimization methods can be divided into two big categories, depending on the process of solution, either deterministic or stochastic optimization methods. A deterministic method of optimization uses the generalized derivative of the objective function, trying to calculate or estimate values of it. On the other hand, the main characteristic of the stochastic methods is that they use random or semi-random searching features, aiming at the optimal solution. Hybrid methods combine features of the two aforementioned categories of methods.

To choose between the two wide categories of optimization methods, the following facts should be considered. The development of a deterministic method is rather time consuming, it is mainly linked to the current problem and cannot easily be expanded to account for other similar problems (i.e. change of objective function), but it converges fast to the solution, having at the same time the risk of being trapped to a local extremum, heavily depending on the initialization of the problem.

On the other hand, stochastic optimization methods can be used like "black boxes" on completely different problems, but they cost much more, because they offer the potential of locating the global optimal solution, independently of the initialization.

The optimization method to be used in this thesis is a gradient-based one.

## 1.3 Literature Review

Tribology research has been extensive during the last decades, focusing on several mechanical components that have an interesting frictional behavior, such as thrust bearings, journal bearings and piston rings. Their performance can be predicted on the basis of the Reynolds equation, which accounts for the physics of the lubricant film that separates the rotor from the stator and takes a wedge-like shape. The fluid slider can take many different shapes such as; simple converging, step (converging or parallel), tapered, parabolic and more modern designs, such as the artificially textured (converging or parallel). A detailed analysis of the geometric characteristics of the lubricating film in tribological contacts, the derivation of the Reynolds equation and the application of the appropriate boundary conditions have been presented in [6].

For a typical slider geometry, quite a few publications exist in the subject of optimization performance of tribological contacts. The load-carrying capacity of a contact, is defined as the integral of the pressure field, computed from Reynolds equation, is the most important performance indicator, which should always be maximum, in order to avoid wear and damage of the two interacting surfaces. Most of publications have studied such geometries, under the scope of the geometry being characterized by a number of parameters and optimized according to these parameters, aiming at the maximization of load-carrying capacity (objective function). Parallel and converging sliders, both plain and textured, and step sliders have been studied in [7], [8] and [9]. All these studies utilize evolutionary algorithms for the purpose of optimization, which is a very strong tool, but does not understand the physics of the problem. This is obviously an advantage, as the optimization algorithm can be applied for many different problems without making any changes but, on the other hand, a disadvantage, because it cannot provide any further information about the effect of design parameters upon the objective function.

This is where gradient based optimization methods become useful. More specifically, adjoint based methods, which is the main interest of the present thesis, compute the sensitivity derivatives of the objective function with respect to the design variables, which express how much the objective function will be altered if a design variable is slightly increased or decreased [5].

In the present study, several converging slider geometries are studied, using an adjoint based optimization method. At first, the slider is parameterized by only one parameter the converging ratio of the slider. In the second method, being also the more interesting one, the design variables are the nodal values of the film thickness, meaning that the geometry is free to take any possible shape. This has been the main motivation for using an adjoint based method, because the geometry is permitted to adjust on its own to the optimal shape, determined by the sensitivity derivatives of the objective function.

## 2. Theoretical Part

The tribology systems studied in this thesis are met in engineering applications and mainly in almost all types of propulsion and energy generation (Diesel) engines and shaft power systems. In Diesel engines, mechanical losses in the form of friction are located in: piston rings pack, guide shoe bearings, main bearings and connecting rod bearings. In a shaft system, and specifically in a ship shaft system, friction is located in the journal bearings (stern-tube and line bearings), in the thrust bearing and in the gearbox units, if one exists. Each mechanical component mentioned above, will be briefly described in the following sections.

## 2.1 Mechanical components

In this section, the several mechanical components where friction is present will be discussed and their geometries will be illustrated.

### 2.1.1   Piston rings

Piston rings are circular metallic rings placed around the piston with a certain pretension, and their main purpose is to isolate the combustion chamber volume with minimum friction. They also transfer heat from the piston to the liner and stabilize the piston so that it is supported symmetrically by the bore. A typical sketch of a piston with its piston rings can be seen in Figure 1, along with a real image of a piston head with the piston rings installed around it.
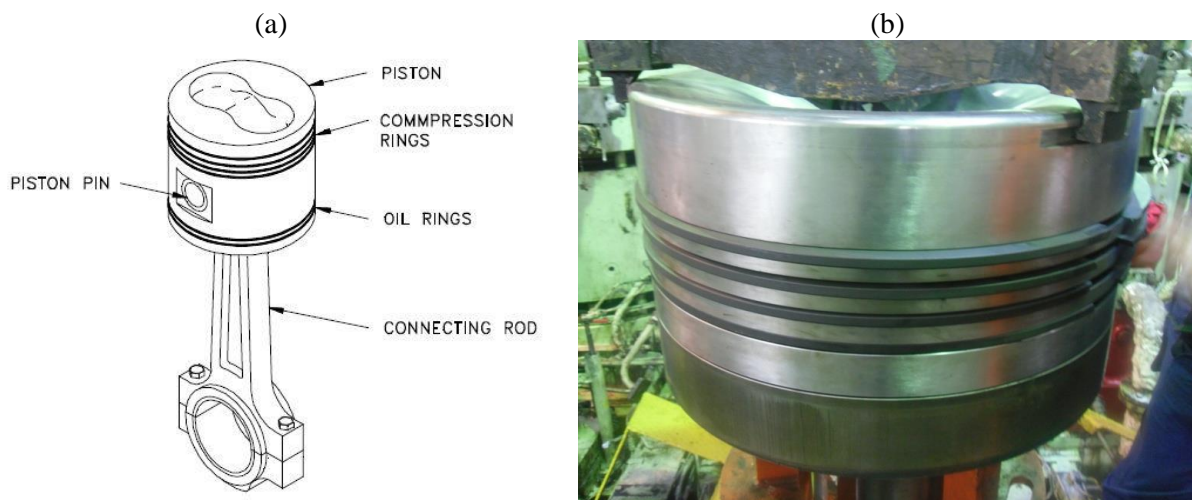


**Figure 1: (a) Piston and its components [13], (b) Piston and the piston rings of M/V Despoina.**

The main purpose of piston rings is to keep gas blow-by from the combustion chamber to the crankcase to a minimum, because leakage will reduce compression pressure and power will be lost. The combustion gases can flow past the piston ring from three locations, the piston ring gap (the gap used to fit the ring around the piston), the front face of the ring and its

backside. Piston rings seal the gas by expanding outwards towards the liner due to the gas pressure acting on their back and the pretension force.

Piston rings also spread the lubricating oil up and down the liner uniformly and at the same time scrape off the excessive oil and return it to the crankcase during the downstroke. These functions are carried out by specially designed oil rings that have a distinguishing face profile geometry.

Another function of piston rings is heat transfer from the piston to the liner. Through the cooling system of the piston head, a part of the combustion heat is transferred to the piston boundaries and, from there, to the piston rings and, finally, to the liner wall.

Piston rings also stabilize the piston, preventing it from coming into contact with the liner, especially during cold starts. While the piston moves along the liner, the piston ring creates a thin lubricating film between it and the liner preventing metal to metal contact. Film thickness is maximum when the piston speed is maximum (middle of a stroke), and minimum when the piston reaches the two centers (top dead center-TDC, bottom dead center-BDC), where contact between surface asperities may occur, making a certain amount of wear inevitable. This fact makes the need of self-lubrication properties of the piston ring and liner materials necessary [10].

### 2.1.2   Journal bearings (based on [6], [11] and [12])

Journal bearings are mechanical components appearing in the majority of engineering applications. They are used either to support the radial load of a rotating shaft or simply as a guide for the smooth transmission of torque with minimum both power loss and wear. The geometry of a journal bearing consists of a hollow cylinder, enclosing a solid shaft that rotates about its axis. The radius of the bearing is slightly larger than that of the shaft; the difference between the bearing and the shaft radius is called clearance. The bearing cylinder is usually held stationary. The hydrodynamic film which supports the radial load is generated between the surfaces of the rotating shaft and the stationary bearing. A typical sketch of a journal bearing during operation, including the developed hydrodynamic film is shown in Figure 2.
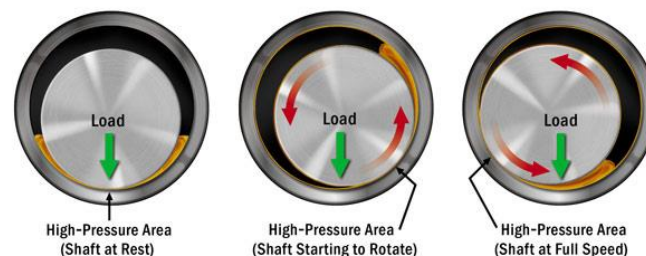


**Figure 2: Journal bearing sketch with the developed oil film (http://www.machinerylubrication.com).**

18

### 2.1.3 Thrust bearings (based on [11])

The hydrodynamic principles used in the lubrication of the two previously mentioned mechanical components are also employed in thrust bearings, which provide axial load support or simply axial load support for a rotor. Fluid-film design can range from coin-sized flat washers to more complicated assemblies several meters in diameter. In all cases, a fluid-film pressure is generated to balance the externally applied thrust load, with proper separation of the two interacting surfaces, in order to prevent material wear, to provide a movement with low friction and to maintain temperature rise in lower levels. Usually, thrust bearing consists of a number of sector-shaped pads, arranged in a shape around the shaft as illustrated in Figure 3, so the external load is equally divided among the pads. Due to the motion of the rotor, the lubricant fluid is drawn inside the wedge-shaped zone and hydrodynamic lubrication occurs, supporting the applied load and preventing metal to metal contact.

(a)                                                                                    (b)
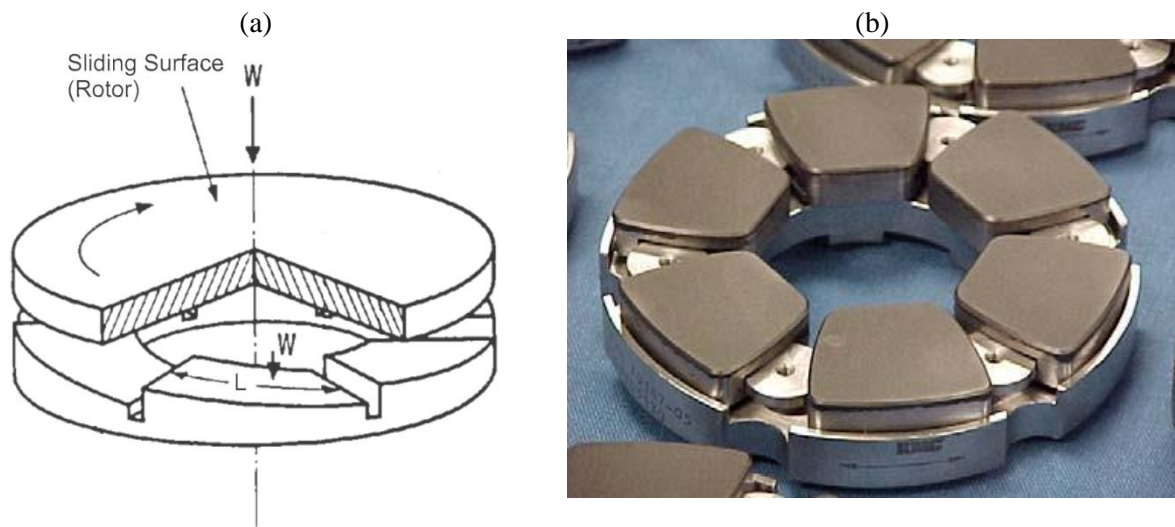


**Figure 3: (a) Sketch of the thrust bearing and the wedge-shaped lubrication zone, (b) Image of a real thrust bearing with six sector-shaped pads.**

## 2.2 Adjoint Optimization

### 2.2.1 Basic Definitions

In section 1.2 the most commonly used optimization methods have been mentioned. Deterministic methods, operating with the derivatives of the objective function, render necessary the use of a technique able to compute the first or even the second derivatives of the objective function.

Despite the vast range of methods being available, for the optimization in problems of fluids flow, it is necessary to employ tools for the computation of the objective function. Such methods are called adjoint methods [5], which is also the method that will be used and properly applied for problems of hydrodynamic lubrication.

Generally, when referring to adjoint methods, it must be clarified that they are mathematical-computational tools for the calculation of the gradient of an objective function, ensuring at the same time the satisfaction of the primal equations governing the problem (i.e. fluid equations). Mathematically, adjoint methods have their roots in the Lagrangian multipliers theory. The computation of the objective function derivatives is useful because they can lead to the solution minimizing (or maximizing) the objective function. Therefore, when referring to an adjoint optimization method, this will also include the process of minimization (or maximization) of the objective function (i.e. steepest descent, conjugate gradient etc.).

In contrast to evolutionary algorithms, any change of the problem and of the objective function, demands the mathematical reformulation of the problem and rewriting of parts of the computational algorithm. [5]

In order to better explain this method, a shape described by a number of geometric parameters, $\vec{b} = [b_1, b_2, ..., b_N]$, located in a fluid domain, should be optimized in order to exhibit minimum drag. The values $b_i$ consisting the vector $\vec{b}$ are called either design or optimization parameters or degrees of freedom (DoFs). Using the adjoint method, for any objective function $F$ and for a certain vector of design variables $\vec{b}_k$ ($n$ marks the current step of optimization), the partial derivatives are:

$$\frac{\partial F}{\partial \vec{b}}(\vec{b}^k) = \left(\frac{\partial F}{\partial b_1}, \frac{\partial F}{\partial b_2}, ..., \frac{\partial F}{\partial b_N}\right)(\vec{b}^k) \tag{1}$$

always assuming that the equations of the primal problem are satisfied.

### 2.2.2  Computational Cost

The main advantage of the adjoint optimization method is that the cost of the computation of the derivatives is almost equal to the cost of the solution of the primal equations. It is also very important that the computational cost is independent of the number of design variables N, in contrast to evolutionary algorithms in which the computational time greatly increases when the design variables are increased. This advantage offsets the need of mathematical reformulation of the problem.

Generally, in hydrodynamic problems the typical way for measuring the computational cost is by considering single evaluation (a single call to the primal equations) as the time unit. The cost of this one solution is analogous to the complexity of the geometry and the assumptions made in the flow model. So, a single optimization cycle of an adjoint-based method, requires one call to the primal equations solver and one call to the solver of the adjoint equation, computing the sensitivity derivatives.

# 3. Hydrodynamic Lubrication

## 3.1 Introduction

Hydrodynamic lubrication is the ability of a viscous fluid to separate two inclined surfaces in relative motion, by developing hydrodynamic pressure in a thin lubricating film that separates the surfaces. This results to low friction forces, decrease in surface temperatures and lower rate of material wear.

In order to achieve hydrodynamic lubrication, a moving surface and availability of oil at the gap entrance. The resulting pressure development is caused by the energy transferred from the moving surface to the lubricating oil and satisfies the conservation of mass because, if no pressure was developed, the flow rate at the domain exit would be lower than the flow rate at the domain inlet.

A sketch of a simple two-dimensional slider is presented in Figure 4. The bottom surface (rotor) moves with velocity U while the top surface (stator) is inclined and fixed, creating a wedge-like gap.
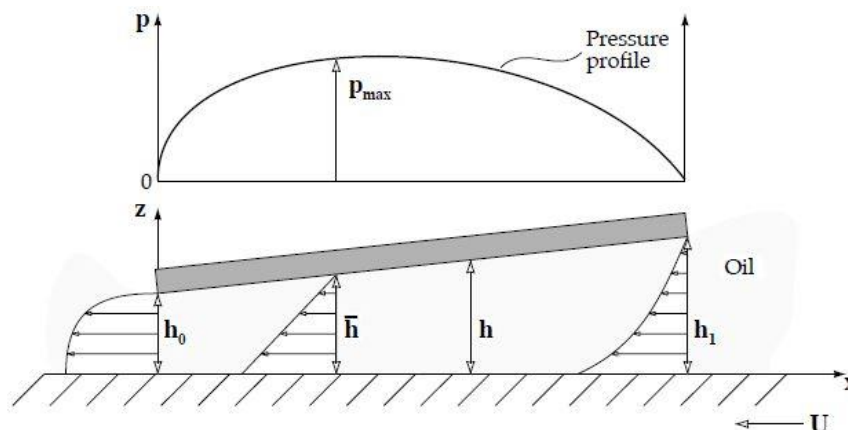


**Figure 4: Hydrodynamic pressure between the inclined surfaces of a simple slider [1].**

Lubricating oil is forced to enter the wedge-shaped gap from the left edge of Figure 4, resulting in increase in its pressure. From the pressure profile of Figure 4, it can be noted that pressure gradient is positive at the inlet, allowing the flow of oil into the wedge, and negative at the outlet, allowing the exit of the oil. Finally, it must be noticed that the transversal profile of fluid velocity depends on the spatial derivative of pressure; at the outlet region, it bends towards the outlet and at the inlet it bends towards the inlet.

The most suitable mathematical equation describing this phenomenon is the Reynolds equation (Osborne Reynolds 1843-1912), which is a simplification of Navier-Stokes equations and can be derived by considering force equilibrium and continuity of flow in an elementary volume of fluid undergoing shear stress.

## 3.2 Simplifying assumptions

In most engineering problems, the processes are too complex and interconnected to be represented by simple mathematical equations. Computers were a real revolution in that respect, as mechanical systems could be analyzed with more detail, taking into account more and more factors.

However, limitations of computational power and time make the use of simpler models inevitable in many cases. In particular, the simplifying assumptions needed for the derivation of the Reynolds equation are the following:

1. The lubricant oil behaves as a Newtonian fluid
2. Inertia forces of the lubricant are neglected
3. Pressure is constant across the thickness of the lubricant fluid
4. Flow is considered as laminar
5. Viscosity is constant in the lubricant domain
6. No-slip condition is employed on the fluid-wall interfaces
7. External body forces acting on the fluid film are neglected

## 3.3 Forces Equilibrium in a finite volume
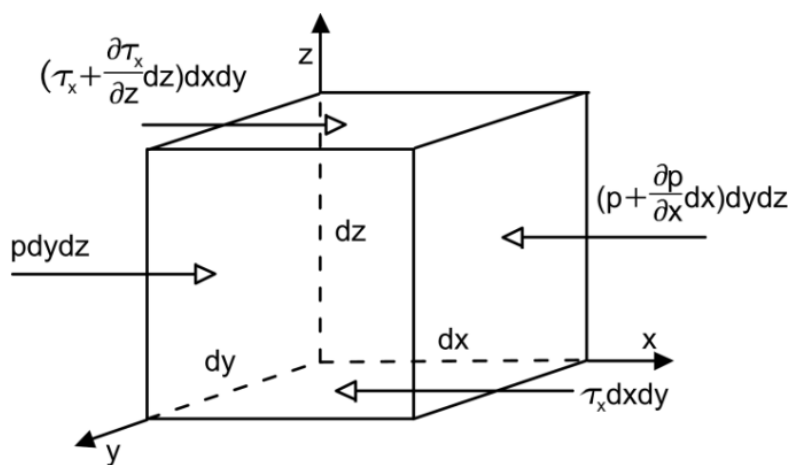


**Figure 5: Force equilibrium of a finite volume of fluid [6].**

A small element of fluid from the lubricating film is considered, as seen in Figure 5, and is assumed that forces are applied only along the x direction. The same results can be extended to the other directions, if needed. Equilibrium of the element dictates that, the forces acting on the left side of the volume must be equal to the forces acting on the right one:

$$pdydz + \left( \tau_x + \frac{\partial \tau_x}{\partial z} dz \right) dxdz = \left( p + \frac{\partial p}{\partial x} dx \right) dydz + \tau_x dxdz \Rightarrow$$

23

$$\frac{\partial \tau_x}{\partial z} dxdydz = \frac{\partial p}{\partial x} dxdydz \tag{2}$$

Considering dxdydz≠0, Eq. (2) can be divided by dxdydz, which yields:

$$\frac{\partial \tau_x}{\partial z} = \frac{\partial p}{\partial x} \tag{3}$$

A similar equation can be derived for the y direction:

$$\frac{\partial \tau_y}{\partial z} = \frac{\partial p}{\partial y} \tag{4}$$

Using assumption 3 the pressure is constant along the z direction, thus:

$$\frac{\partial p}{\partial z} = 0 \tag{5}$$

The shear stress of the lubricant is expressed with the use of dynamic viscosity $\mu$ and the rate of shear along both the x and y directions as follows:

$$\tau_x = \mu \frac{\partial u}{\partial z} \tag{6}$$

$$\tau_y = \mu \frac{\partial v}{\partial z} \tag{7}$$

where, $\tau_x$ and $\tau_y$ are the shear stress acting along the x and y direction, respectively, whereas u, v are the corresponding fluid velocities.

Substituting Eq. (6) into Eq. (3) and Eq. (7) into Eq. (4):

$$\frac{\partial p}{\partial x} = \frac{\partial}{\partial z}\left( \mu \frac{\partial u}{\partial z} \right) \tag{8}$$

$$\frac{\partial p}{\partial y} = \frac{\partial}{\partial z}\left( \mu \frac{\partial v}{\partial z} \right) \tag{9}$$

Integrating Eq. (8) and using the assumption of no-slip conditions (assumption (6.))

$$\frac{\partial p}{\partial x} \frac{z^2}{2} + C_1 z + C_2 = \mu u \tag{10}$$

For the simple slider of Figure 4, the following boundary conditions can be used:

$$u = U_2 \quad \text{at} \quad z = 0 \tag{11}$$

$$u = U_1 \quad \text{at} \quad z = h \tag{12}$$

These conditions are for the general case where the two surfaces move with different velocities $U_1$ and $U_2$; later on, the proper conditions for the case of the present study will be applied.

Substituting the boundary conditions Eq. (11) and Eq. (12) into Eq. (10):

$$C_1 = (U_1 - U_2)\frac{\mu}{h} - \frac{\partial p}{\partial x}\frac{h}{2}$$

$$C_2 = \mu U_2$$

Finally, the equation of velocity of the fluid results from Eq. (10), by substituting the above constants $C_1$ and $C_2$:

$$u = \left(\frac{z^2 - zh}{2\mu}\right)\frac{\partial p}{\partial x} + (U_1 - U_2)\frac{z}{h} + U_2 \tag{13}$$

The equation for the velocity along the y direction can be derived in a similar way:

$$v = \left(\frac{z^2 - zh}{2\mu}\right)\frac{\partial p}{\partial y} + (V_1 - V_2)\frac{z}{h} + V_2 \tag{14}$$

In Eqs. (13) and (14), the three separate terms represent the three velocity profiles that, when combined, give the final velocity profile, see Figure 6.



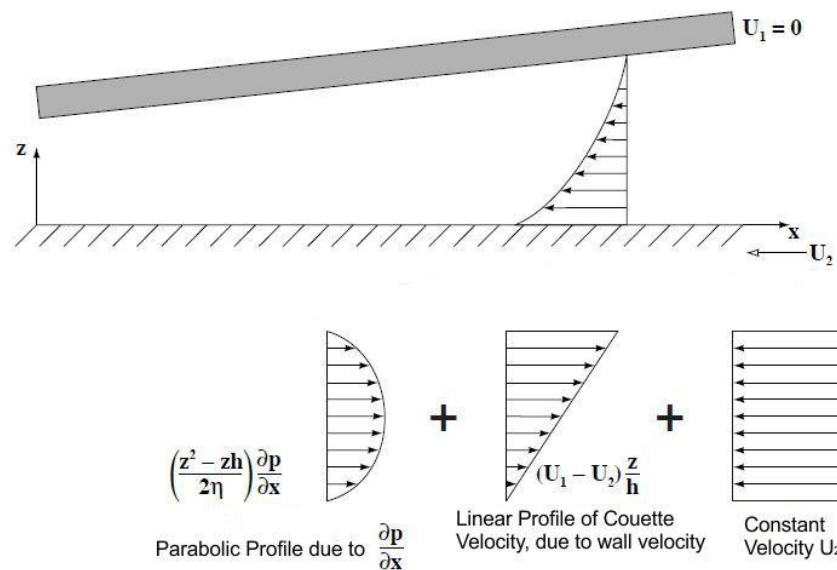**Figure 6: Profiles of the three separate velocity terms at the lubricant inflow region.**

Velocity Assumptions

In most hydrodynamic problems, one of the two surfaces can be considered stationary (stator) and the other one moving with speed U (or/and V) (rotor).

In the present problem, it is assumed that velocity is non-zero only in the x direction, meaning that the velocities $V_1$ and $V_2$ can be taken as zero.

25

As a result, the equations for the two velocities along the x and y directions, respectively, are:

$$u = \left(\frac{z^2 - zh}{2\mu}\right)\frac{\partial p}{\partial x} + -U\frac{z}{h} + U \tag{15}$$

$$v = \left(\frac{z^2 - zh}{2\mu}\right)\frac{\partial p}{\partial y} \tag{16}$$

## 3.4 Continuity of column of fluid

In this section, an infinitesimal volume of the fluid is considered and mass conservation is taken into account. The volume has hexahedral shape and dimensions dx, dy and dz along the three principal axes, as seen in Figure 7. The mass conservation law can be expressed by means of Eq. (17):

$$\left\{\begin{array}{l}\text{Accumulation Rate}\\ \text{of mass in the control}\\ \text{volume}\end{array}\right\} = \left\{\begin{array}{l}\text{Inflow rate of}\\ \text{the control volume}\end{array}\right\} - \left\{\begin{array}{l}\text{Outflow rate of}\\ \text{the control volume}\end{array}\right\} \tag{17}$$

The above values refer to a specific moment in time, so if at a next moment, $t_0$, the mass included in the control volume is ρdxdydz, the first term of Eq. (17) can be written as:

$$\frac{\partial \rho}{\partial t}dxdydz \tag{18}$$

Concerning the calculation of inflow and outflow rates, it is assumed that mass is entering the control volume from the left side (+) and exits from the right (-), as see in Figure 7.
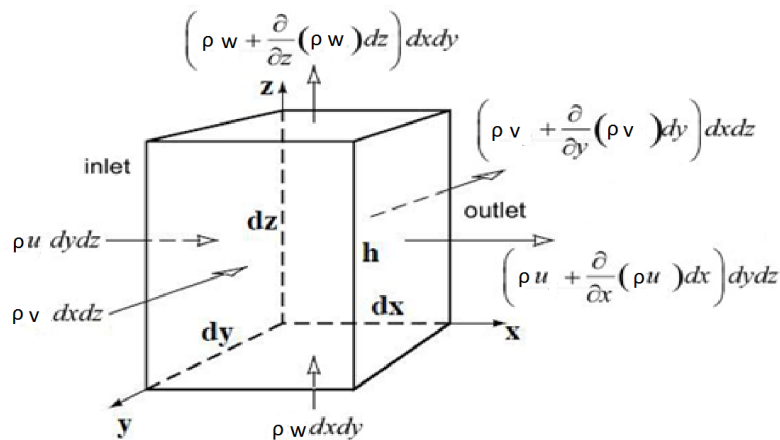


**Figure 7: Continuity of flow in a column of fluid [6].**

26

So inflow rate, from the left side of the finite volume with area dydz, is equal to:

$$\dot{m}_{x,in} = \rho u dy dz \tag{19}$$

The outflow rate, from the right side of the finite volume, is:

$$\dot{m}_{x,out} = \left( \rho u + \frac{\partial}{\partial x}(\rho u) dx \right) dy dz \tag{20}$$

In a similar way, the equations for mass conservation in the y and z directions are:

$$\dot{m}_{y,in} = \rho v dx dz \tag{21}$$

$$\dot{m}_{y,out} = \left( \rho v + \frac{\partial}{\partial y}(\rho v) dy \right) dx dz \tag{22}$$

$$\dot{m}_{z,in} = \rho w dx dy \tag{23}$$

$$\dot{m}_{z,out} = \left( \rho w + \frac{\partial}{\partial z}(\rho w) dz \right) dx dy \tag{24}$$

From Eq. (19)-(24), the right part of Eq. (17) can be written as:

$$\left( \dot{m}_{x,in} + \dot{m}_{y,in} + \dot{m}_{z,in} \right) - \left( \dot{m}_{x,out} + \dot{m}_{y,out} + \dot{m}_{z,out} \right) =$$

$$= -\left( \frac{\partial}{\partial x}(\rho u) + \frac{\partial}{\partial y}(\rho v) + \frac{\partial}{\partial z}(\rho w) \right) dx dy dz \tag{25}$$

Substituting Eq. (18) and (25) into Eq. (17) yields:

$$\left( \frac{\partial \rho}{\partial t} + \frac{\partial}{\partial x}(\rho u) + \frac{\partial}{\partial y}(\rho v) + \frac{\partial}{\partial z}(\rho w) \right) dx dy dz = 0 \tag{26}$$

In Eq. (26), the finite volume dxdydz is non-zero, therefore it can be eliminated:

$$\frac{\partial \rho}{\partial t} + \frac{\partial}{\partial x}(\rho u) + \frac{\partial}{\partial y}(\rho v) + \frac{\partial}{\partial z}(\rho w) = 0 \tag{27}$$

Each term of Eq. (27) will now be integrated along the z direction from 0 to h (film thickness) considering that way a column of fluid instead of a finite volume. The velocities substituted in these terms are taken from Eq. (15) and (16).

$$\int_0^h \frac{\partial}{\partial x}(\rho u)dz = \frac{\partial}{\partial x}\int_0^h \rho u\, dz - \rho u(h)\frac{\partial h}{\partial x} = \frac{\partial}{\partial x}\int_0^h \rho\left[\left(\frac{z^2 - zh}{2\mu}\right)\frac{\partial p}{\partial x} - U\frac{z}{h} + U\right]dz - \rho\left[\left(\frac{h^2 - h\cdot h}{2\mu}\right)\frac{\partial p}{\partial x} - U\frac{h}{\mu} + U\right]\frac{\partial h}{\partial x} =$$

$$= \frac{\partial}{\partial x}\int_0^h \rho\left[\left(\frac{z^2 - zh}{2\mu}\right)\frac{\partial p}{\partial x}\right]dz - \frac{\partial}{\partial x}\int_0^h U\rho\frac{z}{h}dz + \frac{\partial}{\partial x}\int_0^h U\rho\, dz = -\frac{\partial^2 p}{\partial x^2}\frac{\rho}{12\mu}h^3 + \frac{U}{2}\frac{\partial(\rho h)}{\partial x}$$

$$\int_0^h \frac{\partial}{\partial y}(\rho v)dz = \frac{\partial}{\partial y}\int_0^h \rho\left(\frac{z^2 - zh}{2\mu}\right)\frac{\partial p}{\partial y}dz - \rho\left(\frac{h^2 - h\cdot h}{2\mu}\right)\frac{\partial p}{\partial y}\frac{\partial h}{\partial y} = -\frac{\partial^2 p}{\partial y^2}\frac{\rho}{12\mu}h^3$$

$$\int_0^h \frac{\partial}{\partial z}(\rho w)dz = \rho w = \rho\frac{\partial h}{\partial t}$$

$$\int_0^h \frac{\partial \rho}{\partial t}dz = \frac{\partial \rho}{\partial t}h$$

Finally, substituting the above terms in (27), results in Eq. (28) which is the Reynolds equation:

$$-\frac{\partial}{\partial x}\left(\frac{\partial p}{\partial x}\frac{\rho}{12\mu}h^3\right) - \frac{\partial}{\partial y}\left(\frac{\partial p}{\partial y}\frac{\rho}{12\mu}h^3\right) + \frac{U}{2}\frac{\partial(\rho h)}{\partial x} + \frac{\partial(\rho h)}{\partial t} = 0 \tag{28}$$

## 3.5 Assumptions

<u>Constant density</u>
Considering that the fluid density is constant in the lubricant domain, with a value of $\rho_0$ Eq. (21) is simplified as follows:

$$\frac{\partial}{\partial x}\left(\frac{\partial p}{\partial x}\frac{h^3}{12\mu}\right) + \frac{\partial}{\partial y}\left(\frac{\partial p}{\partial y}\frac{h^3}{12\mu}\right) - \frac{U}{2}\frac{\partial h}{\partial x} - \frac{\partial h}{\partial t} = 0 \tag{29}$$

<u>Isoviscous approximation</u>
In many engineering applications the lubricant viscosity is assumed constant throughout the fluid domain. So assuming that viscosity $\mu$=constant, Eq, (29) can further be simplified:

$$\frac{\partial}{\partial x}\left(\frac{\partial p}{\partial x}\frac{h^3}{12}\right) + \frac{\partial}{\partial y}\left(\frac{\partial p}{\partial y}\frac{h^3}{12}\right) - \frac{U\mu}{2}\frac{\partial h}{\partial x} - \frac{\partial h}{\partial t} = 0 \tag{30}$$

## 3.6 Performance parameters of slider

In Figure 8, a sketch of a convergent slider geometry is presented. Using the Reynolds equation (Eq. (29)), the pressure distribution in the lubricant separating the two surfaces can be calculated. Three important performance parameters of this slider mechanism are load capacity (total force acting on the ring in the z-direction), friction force (total force acting on the ring in the x-direction), and friction coefficient, which by definition, is the ratio of friction force to load capacity. Formulaes of calculating those quantities are presented hereinafter.
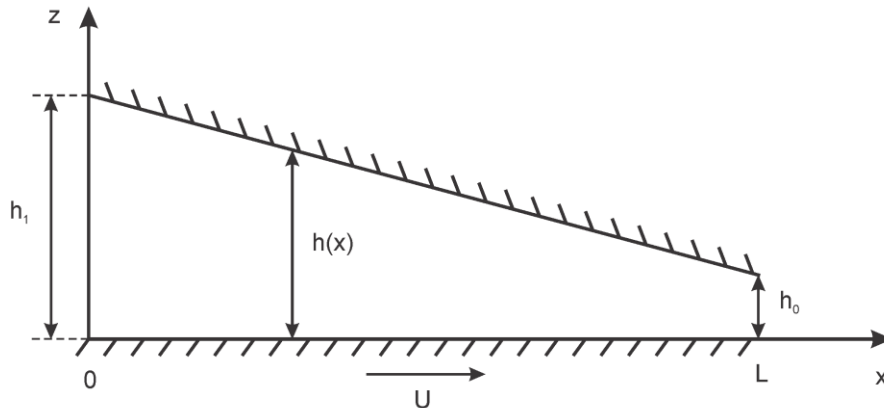


**Figure 8: Sketch of a typical converging slider geometry.**

Load Capacity

The load capacity can be calculated by integrating the pressure distribution along the x-direction:

$$W = \int_0^L p\,dx \tag{31}$$

where L is the length of the slider (see Figure 8)

Friction Force

Friction force can be obtained by integrating the x-component of shear stress along the x-dimension of the slider.

$$F = \int_0^L \tau_x\,dx \tag{32}$$

where $\tau_x$ at the ring-fluid interface can be taken from Eq. (6), and $\partial u\,/\,\partial z$ of Eq. (6) can be easily calculated by differentiating Eq. (13).

According to what is mentioned during the derivation of the Reynolds equation, the shear stress, in terms of dynamic viscosity and velocity, takes the following form:

$$\tau = \mu\frac{du}{dz} \tag{33}$$

where du/dz is easily calculated by differentiating Eq. (13) of velocity u.

After substituting shear stress in the above equation, friction coefficient is given by the following equation:

$$F = \pm \int_0^L \frac{h}{2} \frac{dp}{dx} dx - \int_0^L \frac{U\mu}{h} dx \qquad (34)$$

where, (+) and (-) refer to the friction of the upper and lower surface respectively.

<u>Friction coefficient</u>
Once the load capacity and friction force are known, the friction coefficient, f, can be calculated as:

$$f = \frac{F}{W} \qquad (35)$$

## 3.7 Boundary conditions

In Figure 9, the geometry of a simple convergent-divergent slider is presented. In order to solve the Reynolds equation in the lubricant domain, appropriate boundary conditions need to be described. In the following paragraphs, a description of the boundary conditions mostly used in lubrication problems is given.
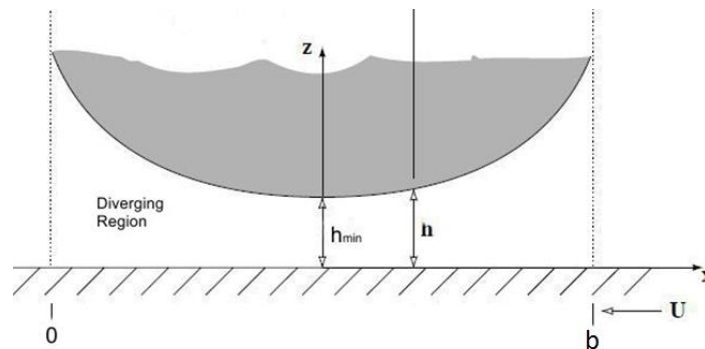


**Figure 9: Sketch of a convergent-divergent slider.**

<u>Full-Sommerfeld Boundary Condition</u>
This boundary condition assumes that pressure is equal to zero at the slider inlet and outlet cross-sections. The pressure distribution for the Full-Sommerfeld boundary condition is presented in Figure 10. Practically, the use of this boundary condition allows the calculation of negative pressures at the diverging region of the slider. In particular, in the diverging part of the slider, pressure distribution is the mirror image of the positive pressure distribution of the converging part of the slider. Overall, the total hydrodynamic load exerted on the slider is zero, which is unrealistic.
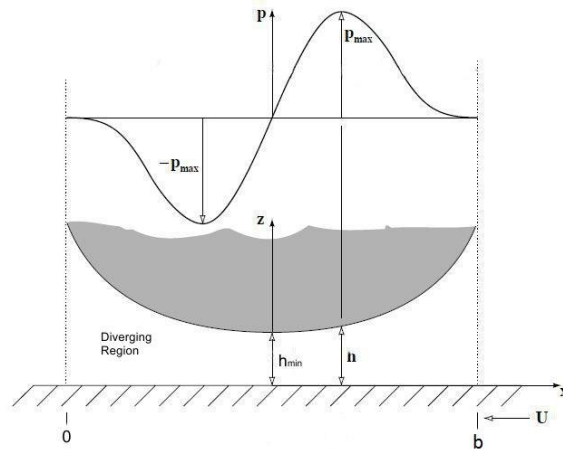
**Figure 10: Solution of the Reynolds equation with Full-Sommerfeld boundary conditions.**

Half-Sommerfeld Boundary Condition

A simple remedy to correct the unrealistic results of the full-Sommerfeld condition is by setting the negative pressures equal to zero. This is the half-Sommerfeld boundary condition and the respective pressure distribution has the form of Figure 11.
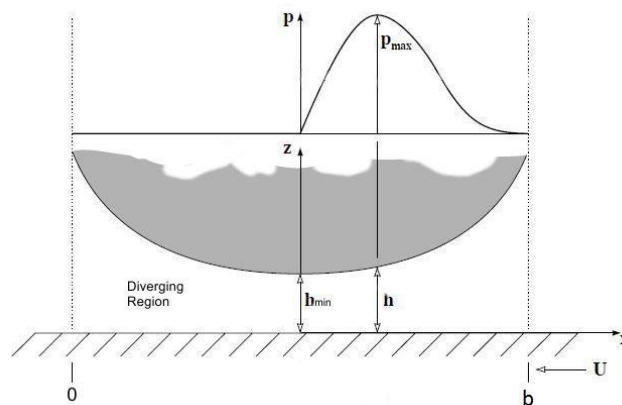


**Figure 11: Solution of the Reynolds equation with Half-Sommerfeld boundary conditions.**

The disadvantage of this boundary condition is that it causes a discontinuity between the pressurized region and the region of zero pressure. Nonetheless, the use of this method is straightforward, and the obtained results are accurate enough for basic engineering use.

Reynolds boundary condition

A better solution to the problem of non-realistic boundary conditions was given by Reynolds, who suggested that negative pressure values should be set equal to zero and that, at the boundary of non-zero and zero pressure, the spatial derivative of pressure should be also equal to zero. The resulting pressure distribution is that of Figure 12.
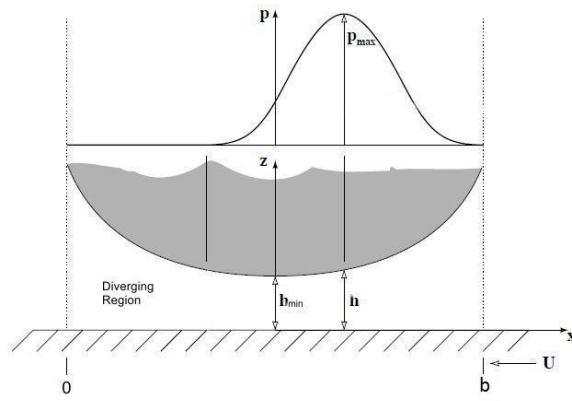
**Figure 12: Solution of the Reynolds equation with Reynolds boundary conditions.**

The Reynolds boundary condition is the one to be used in this thesis.

# 4. Adjoint-based Optimization

The adjoint-based optimization method is applied in a typical convergent slider geometry, which reflects the operation of the majority of tribological contacts. The slider will be modeled in four different ways, based on how the film thickness is defined.

1. One inclined line, the only design variable is the converging ratio $k$.
2. Two consecutive line segments, forming a conveyed and, then, a diverging part; design variables are the two heights of fluid inflow and outflow and the x coordinate of the point where the two lines meet.
3. A step shaped slider, which is described by the inlet height and the position of the step.
4. The film geometry is described by discrete (nodal) values of the thickness distribution; so, the number of design variables is equal to the grid size.

In the first scenario, the optimization aims at the maximization of load capacity and the minimization of friction coefficient, not simultaneously though, while for the rest of the cases the aim is to maximize the load capacity.

## 4.1 One converging line – Maximum Load Capacity

The first one considers the slider as a simple inclined line, characterized by a converging ratio, $k$, and constrained by the minimum value of film thickness, $h_0$. A typical sketch of this geometry is presented in Figure 13.



**Figure 13: Sketch of a typical convergent slider geometry.**

According to Figure 13, the top surface is considered to be the stationary wall (stator), while the bottom surface moves with velocity U, so as to drag the fluid inside the wedge-like converging geometry.

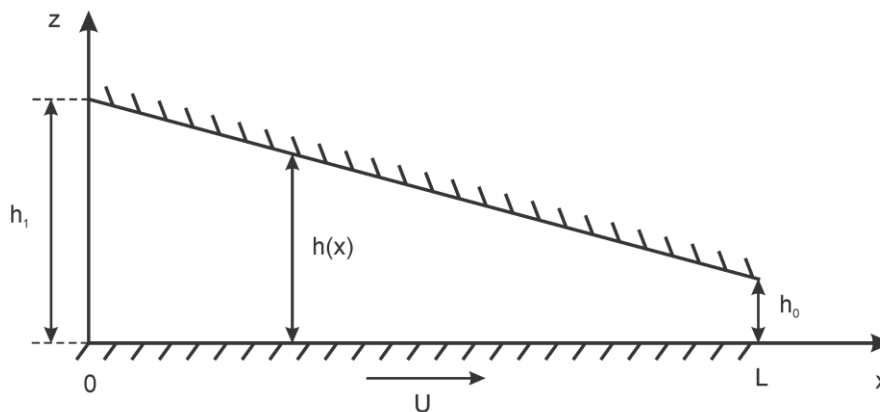A two-dimensional lubricant film separates the two surfaces, spanning in the x-axis. At every point x, the film is characterized by a thickness value h(x).

The inclination of the top surface is defined by two parameters; $h_0$, is the minimum film thickness and is constant. The second parameter (which is the only one which is free) is the converging ratio, $k$; higher values of $k$ correspond to a steepest geometry. Thus, $k$ is the single design variable to be used during the optimization.

### 4.1.1 Primal Problem

The equation governing the primal (flow) problem is the 1-D form of Reynolds equation, as developed in Chapter 3, Eq. (29) and without the time derivative of $h$, or:

$$\frac{d}{dx}\left(\frac{dp}{dx}\frac{h^3}{12}\right) - \frac{U\mu}{2}\frac{dh}{\partial x} = 0 \tag{36}$$

Eq. (36) is solved for the pressure $p$ with an iterative Jacobi solver, after having been discretizing it with a central finite difference scheme. The form to be solved results by expanding the second derivative of the first term, so the final form of Reynolds equation to be used now on is:

$$R = \frac{d^2 p}{dx^2}h^3 + 3h^2\frac{dh}{dx}\frac{dp}{dx} - 6\mu U\frac{dh}{dx} = 0 \tag{37}$$

where $\mu$ is the dynamic viscosity that takes on a constant value throughout the fluid domain, corresponding to a mean temperature between the minimum and maximum temperatures expected within the fluid.

The Reynolds equation (Eq.(37)) is solved along the x-direction and Dirichlet boundary conditions are applied at both ends of the solution domain of constrained length L, as:

$$p(x=0) = p_1$$
$$p(x=L) = p_2$$

The most common choice for pressure values $p_1$ and $p_2$ are to be set equal to zero, representing atmospheric conditions outside the fluid domain. Other constant values can also be considered if the given case demands it.

According to the finite difference method, the spatial derivative of variable $p(i)$ in the x-direction is approximated, following the development of Taylor series:

$$p_{i+1} = p_i + \left.\frac{\partial p}{\partial x}\right|_i \Delta x + \left.\frac{\partial^2 p}{\partial x^2}\right|_i \frac{(\Delta x)^2}{2!} + \left.\frac{\partial^3 p}{\partial x^3}\right|_i \frac{(\Delta x)^3}{3!} + ... + \left.\frac{\partial^n p}{\partial x^n}\right|_i \frac{(\Delta x)^n}{n!} + ...$$

$$p_{i-1} = p_i + \left.\frac{\partial p}{\partial x}\right|_i \Delta x + \left.\frac{\partial^2 p}{\partial x^2}\right|_i \frac{(\Delta x)^2}{2!} - \left.\frac{\partial^3 p}{\partial x^3}\right|_i \frac{(\Delta x)^3}{3!} + ...$$

Considering a small value of $\Delta x$, the higher order terms of the previous equations can be neglected, and the derivative of $p$ at node i can be calculated as:

$$\left.\frac{\partial p}{\partial x}\right|_i = \frac{p_{i+1} - p_{i-1}}{2\Delta x} = \frac{p_{i+1} - p_{i-1}}{x_{i+1} - x_{i-1}}$$

The neglected higher order terms form the error from the exact value (truncation error), therefore, for accurate calculations, an appropriately small value of $\Delta x$ must be selected.

Using the finite difference method described above, each term of Eq. (37) can be discretized with second order accuracy and written in a suitable form, to be solved with a Jacobi iterative process:

$$(37) \Rightarrow \frac{p(i+1) - 2p(i) + p(i-1)}{\Delta x^2} h(i)^3 + 3h(i)^2 \frac{dh}{dx} \frac{p(i+1) - p(i-1)}{2\Delta x} = 6\mu U \frac{dh}{dx}$$

It must be clarified that the term $\dfrac{dh}{dx}$ is not discretized as it can be calculated from the geometry of the current geometry in a closed-form expression. So this is hereafter written as *dhdx(i)*.

Considering that the appropriate form of the above equation is Eq.(38), the expressions for A, B, E and F are separated and imported in an iterative solver:

$$Ap(i+1) + Bp(i-1) + Ep(i) = F \tag{38}$$

$$A = \frac{h(i)^3}{\Delta x^2} + \frac{3h(i)^2 \, dhdx(i)}{2\Delta x}$$

$$B = \frac{h(i)^3}{\Delta x^2} - \frac{3h(i)^2 \, dhdx(i)}{2\Delta x}$$

$$E = -\frac{2h(i)^3}{\Delta x^2}$$

$$F = 6\mu U dhdx(i)$$

Finally, the pressure at any point (i) is computed by solving iteratively Eq. (38) for p(i):

$$p(i) = \frac{F - Ap(i+1) - Bp(i-1)}{E} \tag{39}$$

### 4.1.2 Continuous Adjoint Problem Formulation

The converging ratio is the only variable determining the shape of the lubricant film and is also the design variable of this optimization problem. It is equal to:

$$k = \frac{h_1 - h_0}{h_0} \tag{40}$$

where, $h_0$ is the minimum film thickness, height of outflow, and $h_1$ is the maximum film thickness, height of inflow, see Figure 13.

In most hydrodynamic lubrication cases $h_0$ is a constant parameter of the problem; it is the minimum distance between the top and bottom surfaces and should remain constant during the optimization; as long as $h_0$ is decreased the load capacity carried by the top surface is increased, meaning that infinitesimally small $h_0$ will have the maximum load capacity. Consequently, trying to maximize the load capacity using the minimum film thickness $h_0$, as design variable would result in the trivial solution $h_0=0$.

So, starting from the minimum film thickness $h_0$, $h_1$ can be calculated as:

$$h_1 = (k+1)h_0 \tag{41}$$

and the h(x) value at each node is equal to:

$$h(x) = (k+1)h_0 - \frac{kh_0}{L}x \tag{42}$$

The first derivative of film thickness (*dh/dx*), which appears in the Reynolds equation is now simply equal to the term $\frac{kh_0}{L}$, including the converging ratio $k$.

The function to be maximized is the load capacity of the fluid film, as defined in Eq. (31) which is repeated below:

$$W = \int_0^L p\,dx \tag{43}$$

The sensitivity derivative of the load capacity $W$ with respect to the converging ratio $k$ is computed using the continuous adjoint method as presented in detail below.

At first, the augmented objective function is defined and its derivatives of this are expanded, in order to define the adjoint equation, the adjoint boundary conditions and terms that finally yield the derivative of the objective function with respect to $k$.

Augmented objective function

$$W_{aug} = W + \int_0^L \Psi R dx \qquad (44)$$

where $\Psi$ is the Lagrange multiplier (adjoint variable field) and $R$ is the primal equation residual, which is anyway equal to zero, as shown in Eq. (37).

Derivative of the augmented objective function
In the next step, the derivative of $W_{aug}$ (Eq. (31)), with respect to the vector of the design variables $\vec{b}$ will be developed. The main mathematical tool that will be used is the integration by parts.

$$\frac{\delta W_{aug}}{\delta b} = \frac{\delta W}{\delta b} + \frac{\delta}{\delta b}\int_0^L \Psi R dx = \frac{\delta W}{\delta b} + \frac{\delta}{\delta b}\int_0^L \Psi \left( \underbrace{\frac{d^2 p}{dx^2}h^3}_{A} + \underbrace{3h^2 \frac{dh}{dx}\frac{dp}{dx}}_{B} - \underbrace{6\mu U \frac{dh}{dx}}_{C} \right) dx \qquad (45)$$

$$(A) = \frac{\delta}{\delta b}\int_0^L \Psi \frac{d^2 p}{dx^2}h^3 dx = \int_0^L \Psi \frac{d^2}{dx^2}\left(\frac{\delta p}{\delta b}\right)h^3 dx + \int_0^L \Psi \frac{d^2 p}{dx^2}3h^2 \frac{\delta h}{\delta b}dx =$$

$$\left[\Psi h^3 \frac{d}{dx}\left(\frac{\delta p}{\delta b}\right)\right]_0^L - \int_0^L \frac{d}{dx}\left(\Psi h^3\right)\frac{d}{dx}\left(\frac{\delta p}{\delta b}\right)dx + 3\int_0^L \Psi \frac{d^2 p}{dx^2}h^2 \frac{\delta h}{\delta b}dx =$$

$$\left[\Psi h^3 \frac{d}{dx}\left(\frac{\delta p}{\delta b}\right)\right]_0^L - \left[\frac{d}{dx}\left(\Psi h^3\right)\frac{\delta p}{\delta b}\right]_0^L + \int_0^L \frac{d^2}{dx^2}\left(\Psi h^3\right)\boxed{\frac{\delta p}{\delta b}}dx + 3\int_0^L \Psi \frac{d^2 p}{dx^2}h^2 \frac{\delta h}{\delta b}dx$$

$$(B) = \frac{\delta}{\delta b}\int_0^L \Psi \frac{dp}{dx}3h^2 \frac{dh}{dx}dx = 3\int_0^L \Psi \frac{d}{dx}\left(\frac{\delta p}{\delta b}\right)h^2 \frac{dh}{dx}dx + 3\int_0^L \Psi \frac{dp}{dx}2h \frac{\delta h}{\delta b}\frac{dh}{dx}dx + 3\int_0^L \Psi \frac{dp}{dx}h^2 \frac{\delta}{\delta b}\left(\frac{dh}{dx}\right)dx =$$

$$3\left[\Psi h^2 \frac{dh}{dx}\frac{\delta p}{\delta b}\right]_0^L - 3\int_0^L \frac{d}{dx}\left(\Psi h^2 \frac{dh}{dx}\right)\boxed{\frac{\delta p}{\delta b}}dx + 6\int_0^L \Psi \frac{dp}{dx}h \frac{\delta h}{\delta b}\frac{dh}{dx}dx + 3\int_0^L \Psi \frac{dp}{dx}h^2 \frac{\delta}{\delta b}\left(\frac{dh}{dx}\right)dx$$

$$(C) = \frac{\delta}{\delta b}\int_0^L \Psi \left(-6\mu U \frac{dh}{dx}\right)dx = -6\mu U \int_0^L \Psi \frac{\delta}{\delta b}\left(\frac{dh}{dx}\right)dx$$

$$(D) = \frac{\delta}{\delta b}\int_0^L p dx = \int_0^L \boxed{\frac{\delta p}{\delta b}}dx$$

Adjoint equation
The field adjoint equation is derived by selecting the terms that multiply the derivative of the quantity as for which the primal (Reynolds) equation is solved, which are the terms $\frac{\delta p}{\delta b}$, and setting them equal to zero. These terms are within boxes in the expressions above. So:

$$\frac{d^2}{dx^2}\left(\Psi h^3\right) - 3\frac{d}{dx}\left(\Psi h^2 \frac{dh}{dx}\right) + 1 = 0 \Rightarrow$$

37

$$\boxed{\frac{d^2\Psi}{dx^2}h^3 + 3h^2\frac{dh}{dx}\frac{d\Psi}{dx} + 1 = 0}$$

(46)

Eq. (46) is the adjoint equation, which is solved for $\Psi$, after the solution of the primal (Reynolds) equation.

The solution of the adjoint equation uses the same method as for the primal equation, see Chapter 4.2. The expressions of A, B, E and F are:

$$A = \frac{h(i)^3}{\Delta x^2} + \frac{3h(i)^2 \, dhdx(i)}{2\Delta x}$$

$$B = \frac{h(i)^3}{\Delta x^2} - \frac{3h(i)^2 \, dhdx(i)}{2\Delta x}$$

$$E = -\frac{2h(i)^3}{\Delta x^2}$$

$$F = -1$$

The equation that is to be solved as for $\Psi(i)$ in discrete form becomes:

$$A\Psi(i+1) + B\Psi(i-1) + E\Psi(i) = F$$

Adjoint boundary conditions

In order for equation (46) to be solved, two boundary conditions are necessary at both ends of the solution field, namely at x=0 and x=L. These boundary conditions are derived from the terms of Eq. (45) being inside the [ ] brackets.

$$\left[\Psi h^3 \frac{d}{dx}\left(\frac{\delta p}{\delta b}\right)\right]_0^L - \left[\frac{d}{dx}\left(\Psi h^3\right)\frac{\delta p}{\delta b}\right]_0^L + 3\left[\Psi h^2 \frac{dh}{dx}\frac{\delta p}{\delta b}\right]_0^L =$$

$$\Psi h^3 \frac{d}{dx}\left(\frac{\delta p}{\delta b}\right)\bigg|_{x=L} - \Psi h^3 \frac{d}{dx}\left(\frac{\delta p}{\delta b}\right)\bigg|_{x=0} - \frac{d}{dx}\left(\Psi h^3\right)\frac{\delta p}{\delta b}\bigg|_{x=L} + \frac{d}{dx}\left(\Psi h^3\right)\frac{\delta p}{\delta b}\bigg|_{x=0} +$$

$$3\Psi h^2 \frac{dh}{dx}\frac{\delta p}{\delta b}\bigg|_{x=L} - 3\Psi h^2 \frac{dh}{dx}\frac{\delta p}{\delta b}\bigg|_{x=0}$$

(47)

From the boundary conditions of the primal (Reynolds) equation, the following is valid:

$$p(0) = p_1 \Rightarrow \frac{\delta p}{\delta b}\bigg|_{x=0} = 0$$

$$p(L) = p_2 \Rightarrow \frac{\delta p}{\delta b}\bigg|_{x=L} = 0$$

This means that the four final terms in Eq. (47) are equal to zero. Concerning the two first terms in the same equation, the value of $\frac{d}{dx}\left(\frac{\delta p}{\delta b}\right)$ is unknown, so the term multiplying the unknown term, is set equal to zero, imposing:

$$\left. \Psi h^3 \right|_{x=0} = 0 \atop h(0)^3 \neq 0 \Bigg\} \Rightarrow \boxed{\Psi(0) = 0}$$

$$\left. \Psi h^3 \right|_{x=L} = 0 \atop h(L)^3 \neq 0 \Bigg\} \Rightarrow \boxed{\Psi(L) = 0}$$

These are the adjoint boundary conditions.

### 4.1.3 Sensitivity derivative expression

Up to this point, the primal problem has been solved and the pressure has been computed, along with the values of $\Psi$ that resulted from the solution of the adjoint problem. Consequently, the computation of the derivative of W with respect to b is now possible and it is based in the remaining terms of Eq. (45).

$$\frac{\delta W}{\delta b} = 3 \int_0^L \Psi \frac{d^2 p}{dx^2} h^2 \frac{\delta h}{\delta b} dx + 6 \int_0^L \Psi \frac{dp}{dx} h \frac{\delta h}{\delta b} \frac{dh}{dx} dx +$$

$$3 \int_0^L \Psi \frac{dp}{dx} h^2 \frac{\delta}{\delta b} \left( \frac{dh}{dx} \right) dx - 6 \mu U \int_0^L \Psi \frac{\delta}{\delta b} \left( \frac{dh}{dx} \right) dx$$
(48)

In this section, the optimization uses only one design variable which is the converging ratio of the slider, $\vec{b} = [k]$. <u>Here it must be clarified that using an adjoint method for a problem with only one design variable, there is no computational profit. This is mostly performed as a test case in order to proceed in more complex problems with more design variables.</u>
The profile of film thickness, h(x) is reminded here from Eq. (42), in order to calculate the corresponding derivatives, appearing in Eq. (48).

$$h(x) = (k+1) h_0 - \frac{k h_0}{L} x$$

$$\frac{\delta h}{\delta b} = \frac{\delta h}{\delta k} = h_0 - \frac{h_0}{L} x$$
(49)

$$\frac{\delta}{\delta b} \left( \frac{dh}{dx} \right) = \frac{\delta}{\delta b} \left( \frac{dh}{dx} \right) = -\frac{h_0}{L}$$
(50)

Substituting Eq. (49) and (50) into Eq. (48) it yields:

$$\frac{\delta W}{\delta k} = 3 \int_0^L \Psi \frac{d^2 p}{dx^2} h^2 \left( h_0 - \frac{h_0}{L} x \right) dx + 6 \int_0^L \Psi \frac{dp}{dx} h \left( h_0 - \frac{h_0}{L} x \right) \frac{dh}{dx} dx -$$

$$3 \frac{h_0}{L} \int_0^L \Psi \frac{dp}{dx} h^2 dx + \frac{6 \mu U h_0}{L} \int_0^L \Psi dx$$
(51)

### 4.1.4 Optimization Loop
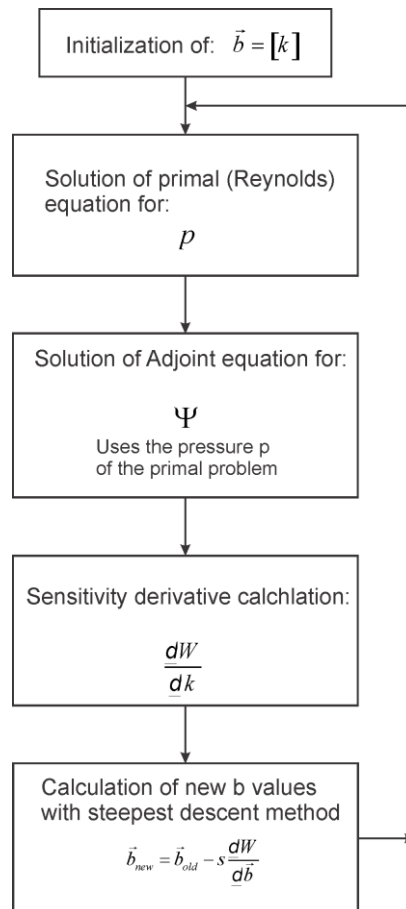


**Figure 14: Optimization flow-chart with the adjoint method.**

The optimization loop starts with the initialization of the design variables, $b$, which for the current case includes only one variable, namely the converging ratio of the slider. Then, the primal problem is solved, using Reynolds equation Eq.(37), and the pressure distribution p is computed. At second, the adjoint equation is solved Eq.(46), using the already computed pressure field. Then, the derivative of the load capacity with respect to the converging ratio is computed, based on Eq.(51). Finally, an updated value of the converging ratio is obtained, with the steepest descent method which uses a step value $s$, appropriately selected, depending on the units of the variables of each case.

### 4.1.5 Results

In this section, the results of the optimization procedure, described in the previous sections are presented and compared with results from the literature.

The optimization has been performed starting from two different initial values of the converging ratio $k$; a very low value, almost k=0, and a high one, k=6. These two bounds of $k$ are selected according to the numerical results of Stachowiak [1], Figure 4.10, page 124.

In Figure 15, the results of the adjoint-based optimization are compared to the diagram of Stachowiak, having in the x-axis the converging ratio and in the y-axis the non-dimensional load multiplied by 6. The non-dimensional load for a 1-D slider is defined as follows:

$$W^* = \frac{W h_0^2}{6 U \mu L^2} \tag{52}$$
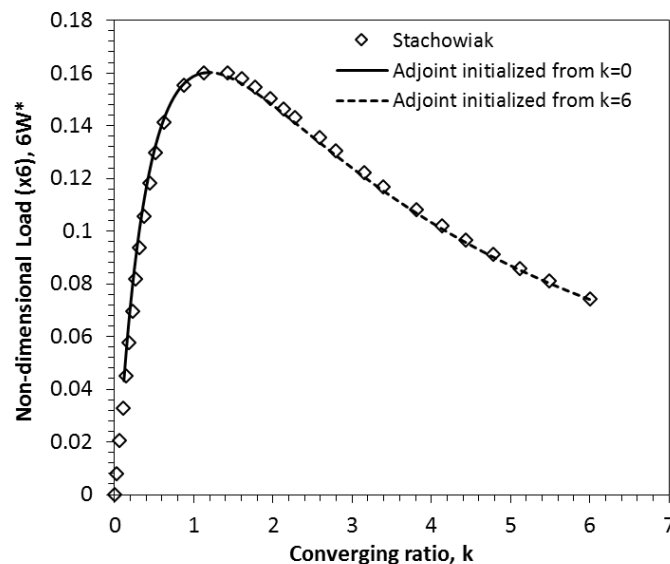


**Figure 15: Comparison between the results of the present study and Stachowiak regarding the non-dimensional load (6W$^*$) [1].**

Starting from k=0, the derivative $\delta W^*/\delta k$ is positive and $W^*$ reaches the maximum value for k=1.2. Similarly, starting from the other side of x-axis, the curve moves to the opposite direction, $\delta W^*/\delta k$ is negative, and the procedure stops at the same point of maximum $W^*$.

From Figure 15, a very good match is observed between the adjoint method of the present study and the relation between W* and k already been presented in [1].

Consequently, considering a simple converging slider, a slider with a converging ratio equal to 1.2 has the maximum load capacity. Lower or higher values of $k$ lead to a decreased load capacity.

## 4.2 One converging line – Minimum Friction Coefficient

In this section, the objective function is the friction coefficient and the design variable will remain the same as that of Section 4.1.

### 4.2.1 Primal Problem

The primal problem is the same as the previous case of Chapter 4.1, and it will also remain the same throughout the following cases. The governing equation is repeated:

$$R = \frac{d^2 p}{dx^2} h^3 + 3h^2 \frac{dh}{dx} \frac{dp}{dx} - 6\mu U \frac{dh}{dx} = 0 \tag{53}$$

### 4.2.2 Adjoint Problem

The function to be minimized is the friction coefficient, Eq. (35).

The friction force is given from Eq. (34). The friction of the lower surface (rotor) is selected as this is the higher than the friction force of the upper surface (stator). So, the objective function of friction coefficient is given by:

$$f = \frac{\int_0^L \left( -\frac{h}{2} \frac{dp}{dx} - \frac{U\mu}{h} \right) dx}{\int_0^L p \, dx} \tag{54}$$

The augmented friction coefficient is:

$$f_{aug} = f + \int_0^L \Psi R \, dx \tag{55}$$

and its derivative is:

$$\frac{\delta f_{aug}}{\delta \vec{b}} = \frac{\delta f}{\delta b} + \frac{\delta}{\delta b} \int_0^L \Psi R \, dx \tag{56}$$

Comparing Eq. (56) and (45), the only change is the derivative $\delta f / \delta b$, which has to be expanded.

$$\frac{\delta f}{\delta b} = \frac{\frac{\delta F}{\delta b} W - F \frac{\delta W}{\delta b}}{W^2} \tag{57}$$

The term $\delta W / \delta b$ has already been calculated during the development of Eq. (45). So:

$$\frac{\delta F}{\delta b} = \frac{\delta}{\delta b} \int_0^L \left( -\frac{h}{2}\frac{dp}{dx} - \frac{U\mu}{h} \right) dx = -\frac{1}{2}\int_0^L \frac{dp}{dx}\frac{\delta h}{\delta b} dx - \frac{1}{2}\int_0^L h \frac{d}{dx}\left( \frac{\delta p}{\delta b} \right) dx - \mu U \int_0^L \frac{\delta}{\delta b}\left( \frac{1}{h} \right) dx =$$

$$-\frac{1}{2}\int_0^L \frac{dp}{dx}\frac{\delta h}{\delta b} dx - \frac{1}{2}\left[ h\frac{\delta p}{\delta b} \right]_0^L + \frac{1}{2}\int_0^L \frac{dh}{dx}\frac{\delta p}{\delta b} dx + \mu U \int_0^L \frac{1}{h^2}\frac{\delta h}{\delta b} dx$$

According to the boundary conditions applying to the pressure field:

$$p(0) = p_1 \Rightarrow \left.\frac{\delta p}{\delta b}\right|_{x=0} = 0$$

, consequently:

$$p(L) = p_2 \Rightarrow \left.\frac{\delta p}{\delta b}\right|_{x=L} = 0$$

$$\frac{\delta F}{\delta b} = -\frac{1}{2}\int_0^L \frac{dp}{dx}\frac{\delta h}{\delta b} dx + \frac{1}{2}\int_0^L \frac{dh}{dx}\frac{\delta p}{\delta b} dx + \mu U \int_0^L \frac{1}{h^2}\frac{\delta h}{\delta b} dx \qquad (58)$$

Going back to Eq. (57), having derived the derivative of friction force, it yields:

$$\frac{\delta f}{\delta b} = \frac{1}{W^2}\left[ -\frac{W}{2}\int_0^L \frac{dp}{dx}\frac{\delta h}{\delta b} dx + \frac{W}{2}\int_0^L \frac{dh}{dx}\frac{\delta p}{\delta b} dx + W\mu U \int_0^L \frac{1}{h^2}\frac{\delta h}{\delta b} dx - F\int_0^L \frac{\delta p}{\delta b} dx \right] =$$

$$= -\frac{1}{2W}\int_0^L \frac{dp}{dx}\frac{\delta h}{\delta b} dx + \frac{1}{2W}\int_0^L \frac{dh}{dx}\boxed{\frac{\delta p}{\delta b}} dx + \frac{\mu U}{W}\int_0^L \frac{1}{h^2}\frac{\delta h}{\delta b} dx - \frac{F}{W^2}\int_0^L \boxed{\frac{\delta p}{\delta b}} dx \qquad (59)$$

In order not to repeat all the previously presented equations, the terms of equation (59) replace the term $\delta W/\delta b$ of Eq. (45), and the rest of the expanded form of Eq. (45) remains the same. Following the same process as in section 4.1.2, the adjoint equation, the adjoint boundary conditions and the sensitivity derivative expression0020are derived.

Adjoint equation

The adjoint equation is partially the same as in Eq. (46), but replacing the third term, which was equal to 1, with the new terms appearing due to the terms within boxes in Eq. (59).

$$\frac{d^2\Psi}{dx^2}h^3 + 3h^2\frac{dh}{dx}\frac{d\Psi}{dx} + \frac{1}{2W}\frac{dh}{dx} - \frac{F}{W^2} = 0 \qquad (60)$$

The solution of the adjoint equation follows the same method as the solution of the primal equation, already presented in Chapter 4.2. The expressions of A', B', E' and F' are:

$$A' = \frac{h(i)^3}{\Delta x^2} + \frac{3h(i)^2 \, dhdx(i)}{2\Delta x}$$

$$B' = \frac{h(i)^3}{\Delta x^2} - \frac{3h(i)^2 \, dhdx(i)}{2\Delta x}$$

$$E' = -\frac{2h(i)^3}{\Delta x^2}$$

$$F' = -\frac{1}{2W}\frac{dh}{dx} + \frac{F}{W^2}$$

Adjoint boundary conditions

They are also the same as in section 4.1.2, while no new constant terms have been added during the development of the above equations. So:

$$\Psi(0) = 0$$

$$\Psi(L) = 0$$

### 4.2.3 Sensitivity derivative expression

In order to derive the expression of the adjoint derivative, the left over terms in Eq. (59) must be added to the terms of Eq. (48). So:

$$\frac{\delta f}{\delta b} = 3\int_0^L \Psi \frac{d^2 p}{dx^2} h^2 \frac{\delta h}{\delta b} dx + 6\int_0^L \Psi \frac{dp}{dx} h \frac{\delta h}{\delta b}\frac{dh}{dx} dx +$$

$$3\int_0^L \Psi \frac{dp}{dx} h^2 \frac{\delta}{\delta b}\left(\frac{dh}{dx}\right) dx - 6\mu U \int_0^L \Psi \frac{\delta}{\delta b}\left(\frac{dh}{dx}\right) dx - \qquad (61)$$

$$-\frac{1}{2W}\int_0^L \frac{dp}{dx}\frac{\delta h}{\delta b} dx + \frac{\mu U}{W}\int_0^L \frac{1}{h^2}\frac{\delta h}{\delta b} dx$$

And because b=k, and while the terms $\dfrac{\delta h}{\delta b}$ are already known from Eq. (49), the final form of the sensitivity derivative is:

$$\frac{\delta f}{\delta k} = 3\int_0^L \Psi \frac{d^2 p}{dx^2} h^2 \left(h_0 - \frac{h_0}{L}x\right) dx + 6\int_0^L \Psi \frac{dp}{dx} h\left(h_0 - \frac{h_0}{L}x\right)\frac{dh}{dx} dx -$$

$$3\frac{h_0}{L}\int_0^L \Psi \frac{dp}{dx} h^2 dx + \frac{6\mu U h_0}{L}\int_0^L \Psi dx \qquad (62)$$

$$-\frac{1}{2W}\int_0^L \frac{dp}{dx}\left(h_0 - \frac{h_0}{L}x\right) dx + \frac{\mu U}{W}\int_0^L \frac{1}{h^2}\left(h_0 - \frac{h_0}{L}x\right) dx$$

### 4.2.4 Results

The optimization loop is the same as that described in the flow-chart of Figure 14; the only difference is that the computed sensitivity derivatives are these of friction coefficient, $f$, with respect to the converging ratio $k$, using Eq.(62). In this section, the results of the optimization procedure are presented and compared with results from the literature.

Similarly to the previous chapter, according to Stachowiak [1] the initialization starts from two different starting points that of k=0 and k=6.

In Figure 16, the results of the adjoint optimization method are compared to the diagram of Stachowiak, having in the x-axis the converging ratio and in the y-axis the non-dimensional friction coefficient, which is given by the following equation:
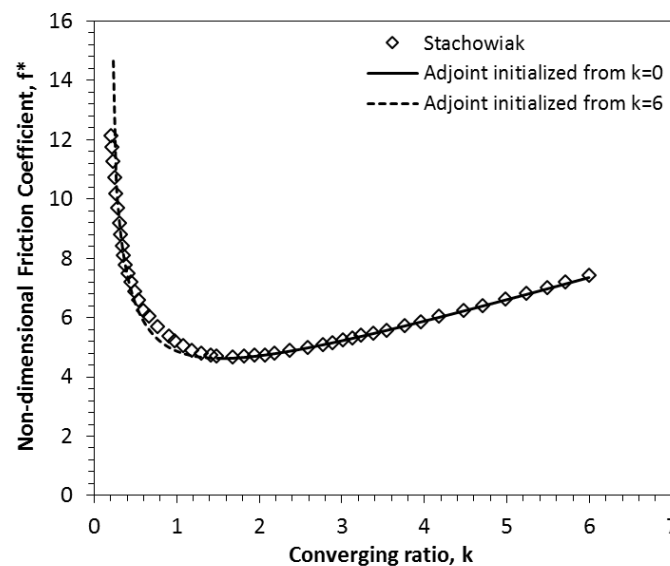
$$f^* = f \frac{L}{h_0} \tag{63}$$



**Figure 16: Comparison between the results of present study and Stachowiak regarding the non-dimensional friction coefficient ($f^*$) [1].**

Starting from k=0, the derivative $\delta f^*/\delta k$ is negative and $f^*$ reaches the minimum value for k=1.55. Similarly, starting from the other side of x-axis, the curve moves to the opposite direction, $\delta f^*/\delta k$ is positive, and the procedure stops at the same point of minimum $f^*$.

From Figure 16, a very good match is observed between the adjoint method of the present study and the relation between f* and k already been presented in [1].

Consequently, considering a simple converging slider, a slider with a converging ratio equal to 1.55 has the minimum friction coefficient. Lower or higher values of $k$ lead to an increased friction coefficient.

## 4.3 Two line segments – Maximum Load Capacity

In the present section, the slider geometry under optimization is that presented in Figure 17, consisting of a converging and a diverging part. The thickness is described by a linear equation, based on the position of the three point, A, inlet area, C, outlet area and B, being the connecting point between the two lines.
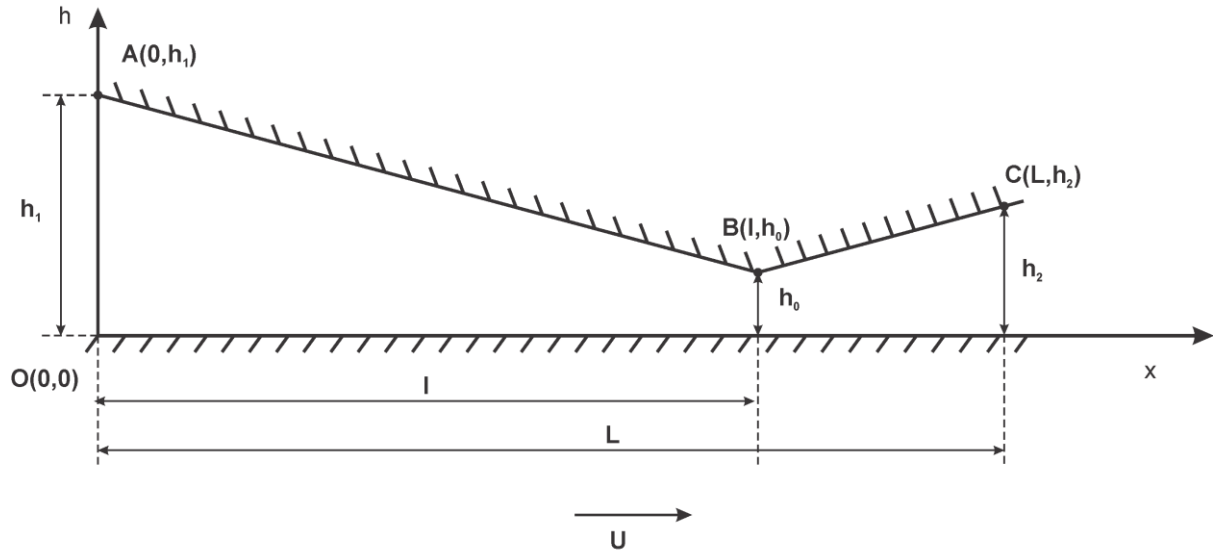


**Figure 17: Lubricated slider consisting of two lines.**

### 4.3.1 Primal Problem

The primal problem is governed by Reynolds equation, as already seen in Eq. (37).

$$R = \frac{d^2 p}{dx^2} h^3 + 3h^2 \frac{dh}{dx}\frac{dp}{dx} - 6\mu U \frac{dh}{dx} = 0 \tag{64}$$

### 4.3.2 Adjoint Problem

The adjoint equation is the same as the previous problem, as the adjoint equation has been derived generally for any vector of design variables b. The adjoint equation is:

$$\frac{d^2 \Psi}{dx^2} h^3 + 3h^2 \frac{dh}{dx}\frac{d\Psi}{dx} + 1 = 0 \tag{65}$$

where $\Psi$ is the adjoint variable.

Similarly, the adjoint boundary conditions remain the same, namely:

$$\Psi(0) = 0$$
$$\Psi(L) = 0$$

### 4.3.3 Sensitivity Derivatives

$$\frac{\delta W}{\delta \vec{b}} = 3\int_0^L \Psi \frac{d^2 p}{dx^2} h^2 \frac{\delta h}{\delta \vec{b}} dx + 6\int_0^L \Psi \frac{dp}{dx} h \frac{\delta h}{\delta \vec{b}} \frac{dh}{dx} dx +$$

$$3\int_0^L \Psi \frac{dp}{dx} h^2 \frac{\delta}{\delta \vec{b}}\left(\frac{dh}{dx}\right) dx - 6\mu U \int_0^L \Psi \frac{\delta}{\delta \vec{b}}\left(\frac{dh}{dx}\right) dx$$

(66)

In Eq. (66) the terms inside the integrals, except the $\delta/\delta b$ terms, are substituted by the following symbols, for the purpose of simplicity:

$$Q_1 = 3\Psi \frac{d^2 p}{dx^2} h^2 + 6\Psi \frac{dp}{dx} h \frac{dh}{dx}$$

$$Q_2 = 3\Psi \frac{dp}{dx} h^2 - 6\eta U \Psi$$

So, Eq. (66) can be rewritten as:

$$\frac{\delta W}{\delta b} = \int_0^L Q_1 \frac{\delta h}{\delta b} dx + \int_0^L Q_2 \frac{\delta}{\delta b}\left(\frac{dh}{dx}\right) dx$$

(67)

At this point, the equations describing the two lines of Figure 17 should be written. Line AB will be resulted knowing that points A and B belong to the line and similarly line BC with the points B and C. Consequently:

Line AB: $h_{AB}(x) = \dfrac{h_0 - h_1}{l} x + h_1$

Line BC: $h_{BC}(x) = \dfrac{h_2 - h_0}{L-l} x + \dfrac{h_0 L - h_2 l}{L-l}$

In order to avoid the non-continuity problems of a step function, a sigmoidal function is defined, describing the whole geometry and exhibiting a small curvature at the connection point B($l,h_0$). The curvature magnitude is controlled by giving different values to the variable $m$ (as seen in the following equations), higher values of $m$ lead to a steeper angle, closer to the real geometry, while lower values of $m$ lead to a more curving geometry.

$$h = \varphi \cdot h_{AB} + (1-\varphi) \cdot h_{BC}$$

(68)

$$\varphi = \varphi(x,l) = \frac{1}{1 + e^{m(x-l)}}$$

(69)

$$h_{AB} = \frac{h_0 - h_1}{l} x + h_1$$

(70)

$$h_{BC} = \frac{h_2 - h_0}{L-l} x + \frac{h_0 L - h_2 l}{L-l}$$

(71)

Substituting Eq. (69), (70) and (71) into Eq. (68) the fluid film geometry is as follows:

$$h(x,l) = \frac{1}{1+e^{m(x-l)}}\left(\frac{h_0 - h_1}{l}x + h_1\right) + \left(1 - \frac{1}{1+e^{m(x-l)}}\right)\left(\frac{h_2 - h_0}{L-l}x + \frac{h_0 L - h_2 l}{L-l}\right) \qquad (72)$$

For this problem the design variables are: $\vec{b} = [h_1, h_2, l]$

According to Eq. (66) the derivatives $\dfrac{\delta h}{\delta \vec{b}} = \left[\dfrac{\delta h}{\delta h_1}, \dfrac{\delta h}{\delta h_2}, \dfrac{\delta h}{\delta l}\right]$ and

$\dfrac{\delta}{\delta \vec{b}}\left(\dfrac{dh}{dx}\right) = \left[\dfrac{\delta}{\delta h_1}\left(\dfrac{dh}{dx}\right), \dfrac{\delta}{\delta h_2}\left(\dfrac{dh}{dx}\right), \dfrac{\delta}{\delta l}\left(\dfrac{dh}{dx}\right)\right]$ should be calculated in order to find the

derivative $\dfrac{\delta W}{\delta b}$ at each optimization step.

➤ $$\frac{\delta h}{\delta l} = \frac{\delta \varphi}{\delta l}h_{AB} + \varphi\frac{\delta h_{AB}}{\delta l} + \frac{\delta h_{BC}}{\delta l} - \frac{\delta \varphi}{\delta l}h_{BC} - \varphi\frac{\delta h_{BC}}{\delta l} \qquad (73)$$

- $\dfrac{\delta \varphi}{\delta l} = \dfrac{me^{m(x-l)}}{\left(1+e^{m(x-l)}\right)^2}$

- $\dfrac{\delta h_{AB}}{\delta l} = \dfrac{h_1 - h_0}{l^2}x$

- $\dfrac{\delta h_{BC}}{\delta l} = \dfrac{\left(h_0 - h_2\right)}{\left(L-l\right)^2}$

➤ $\dfrac{\delta}{\delta l}\left(\dfrac{dh}{dx}\right) = \dfrac{d}{dx}\left(\dfrac{\delta h}{\delta l}\right) = \dfrac{d}{dx}\left(\dfrac{\delta \varphi}{\delta l}\right)h_{AB} + \dfrac{\delta \varphi}{\delta l}\dfrac{dh_{AB}}{dx} + \dfrac{d\varphi}{dx}\dfrac{\delta h_{AB}}{\delta l} + \varphi\dfrac{d}{dx}\left(\dfrac{\delta h_{AB}}{\delta l}\right) + \dfrac{d}{dx}\left(\dfrac{\delta h_{BC}}{\delta l}\right)$

$\qquad - \dfrac{d}{dx}\left(\dfrac{\delta \varphi}{\delta l}\right)h_{BC} - \dfrac{\delta \varphi}{\delta l}\dfrac{dh_{BC}}{dx} - \dfrac{d\varphi}{dx}\dfrac{\delta h_{BC}}{\delta l} - \varphi\dfrac{d}{dx}\left(\dfrac{\delta h_{BC}}{\delta l}\right)$

- $\dfrac{d\varphi}{dx} = -\dfrac{me^{m(x-l)}}{\left(1+e^{m(x-l)}\right)^2}$

- $\dfrac{d}{dx}\left(\dfrac{\delta \varphi}{\delta l}\right) = \dfrac{m^2 e^{m(x-l)}}{\left(1+e^{m(x-l)}\right)^2} - \dfrac{2m^2 e^{2m(x-l)}}{\left(1+e^{m(x-l)}\right)^3}$

- $\dfrac{dh_{AB}}{dx} = \dfrac{h_0 - h_1}{l}$

- $\dfrac{d}{dx}\left(\dfrac{\delta h_{AB}}{\delta l}\right) = \dfrac{h_1 - h_0}{l^2}$

- $\dfrac{dh_{BC}}{dx} = \dfrac{h_2 - h_0}{L-l}$

- $\dfrac{d}{dx}\left(\dfrac{\delta h_{BC}}{\delta l}\right) = \dfrac{h_2 - h_0}{\left(L-l\right)^2}$

➤ $\dfrac{\delta h}{\delta h_1} = \cancel{\dfrac{\delta\varphi}{\delta h_1}}^{0} h_{AB} + \varphi\dfrac{\delta h_{AB}}{\delta h_1} + \cancel{\dfrac{\delta h_{BC}}{\delta h_1}}^{0} - \cancel{\dfrac{\delta\varphi}{\delta h_1}}^{0} h_{BC} - \varphi\cancel{\dfrac{\delta h_{BC}}{\delta h_1}}^{0} = \varphi\dfrac{\delta h_{AB}}{\delta h_1}$

- $\dfrac{\delta h_{AB}}{\delta h_1} = -\dfrac{1}{l}x + 1$

➤ $\dfrac{\delta}{\delta h_1}\left(\dfrac{dh}{dx}\right) = \dfrac{d}{dx}\left(\dfrac{\delta h}{\delta h_1}\right) = \dfrac{d\varphi}{dx}\dfrac{\delta h_{AB}}{\delta h_1} + \varphi\dfrac{\delta}{\delta h_1}\left(\dfrac{dh_{AB}}{dx}\right)$

- $\dfrac{\delta}{\delta h_1}\left(\dfrac{dh_{AB}}{dx}\right) = -\dfrac{1}{l}$

➤ $\dfrac{\delta h}{\delta h_2} = \cancel{\dfrac{\delta\varphi}{\delta h_2}}^{0} h_{AB} + \varphi\cancel{\dfrac{\delta h_{AB}}{\delta h_2}}^{0} + \dfrac{\delta h_{BC}}{\delta h_2} - \cancel{\dfrac{\delta\varphi}{\delta h_2}}^{0} h_{BC} - \varphi\dfrac{\delta h_{BC}}{\delta h_2} = \left(1-\varphi\right)\dfrac{\delta h_{BC}}{\delta h_2}$

- $\dfrac{\delta h_{BC}}{\delta h_2} = \dfrac{1}{L-l}x - \dfrac{l}{L-l}$

➤ $\dfrac{\delta}{\delta h_2}\left(\dfrac{dh}{dx}\right) = \dfrac{d}{dx}\left(\dfrac{\delta h}{\delta h_2}\right) = \left(1-\varphi\right)\dfrac{\delta}{\delta h_2}\left(\dfrac{dh_{BC}}{dx}\right) - \dfrac{d\varphi}{dx}\dfrac{\delta h_{BC}}{\delta h_2}$

- $\dfrac{\delta}{\delta h_2}\left(\dfrac{dh_{BC}}{dx}\right) = \dfrac{1}{L-l}$

Finally, an external constraint is implemented upon the solution, setting the values of film thickness that are lower than $h_{min}$, equal to $h_{min}$.


### 4.3.4 Results

Having computed the sensitivity derivative of W, using Eq. (67), the optimization loop can be initiated, as already presented in Figure 14. Several runs have been performed, starting from different initialization points. Especially, three different initializations have been selected, almost equally distributed within the fluid film region, as follows:

1. $h_1 = 100$ μm, $h_2 = 60$ μm, $l = 0.035$

**Figure 18: Non-dimensional load capacity trend along the optimization loop, $W^*_{opt}$=0.32055.**

The initial geometry and the optimal geometry are presented in Figure 19.



**Figure 19: Initial and final geometry of lubricant film geometry. Optimal values of the design variables are: $[h_1, h_2, l]$ = [0.000112, 0.00005, 0.040073].**

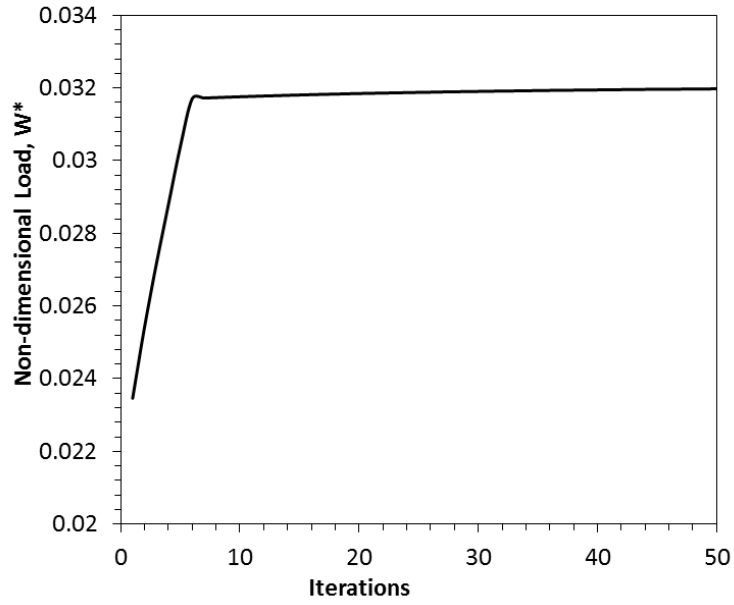2. $h_1 = 80$ μm, $h_2 = 60$ μm, $l = 0.015$



**Figure 20: Non-dimensional load capacity trend along the optimization loop, $W^*_{opt}$=0.32055.**

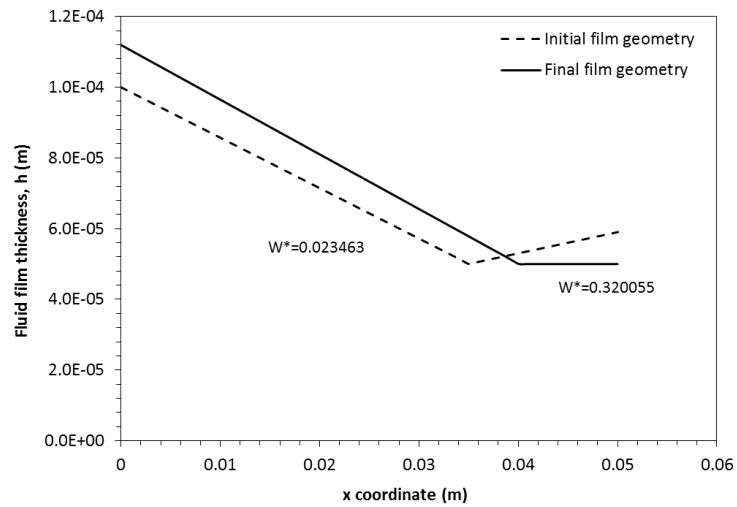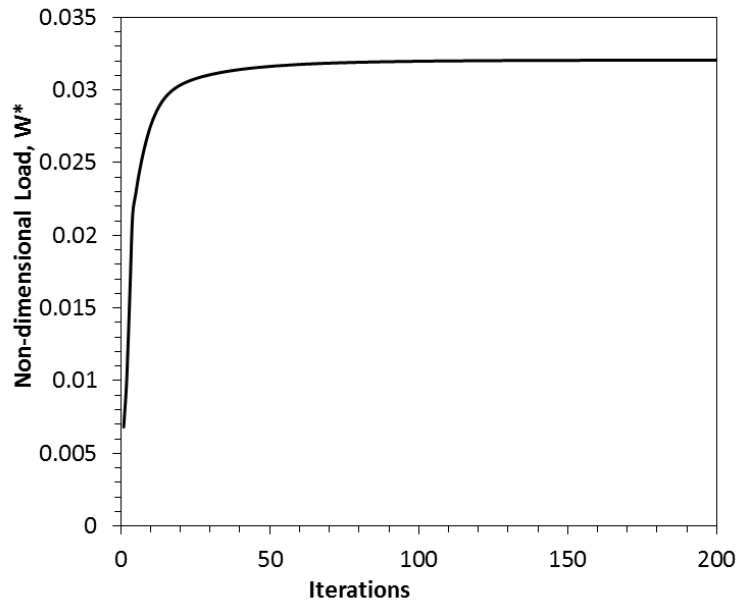The initial geometry and the optimal geometry are presented in Figure 21.



**Figure 21: Initial and final geometry of lubricant film geometry. Optimal values of the design variables are: $[h_1, h_2, l] = [0.000112, 0.00005, 0.040073]$.**

3. $h_1 = 130$ μm, $h_2 = 60$ μm, $l = 0.025$



**Figure 22: Non-dimensional load capacity evolution along the optimization loop, $W^*_{opt}$=0.032055.**

The initial geometry and the final geometry after the optimization procedure are presented in Figure 23.
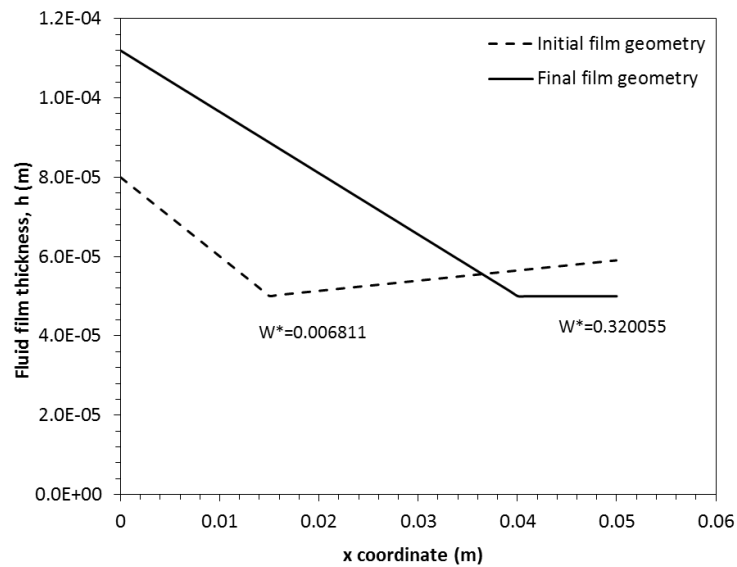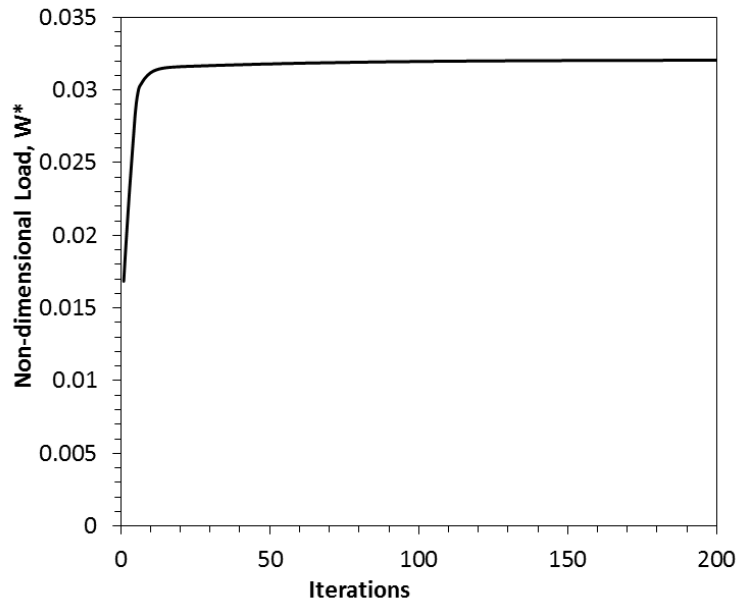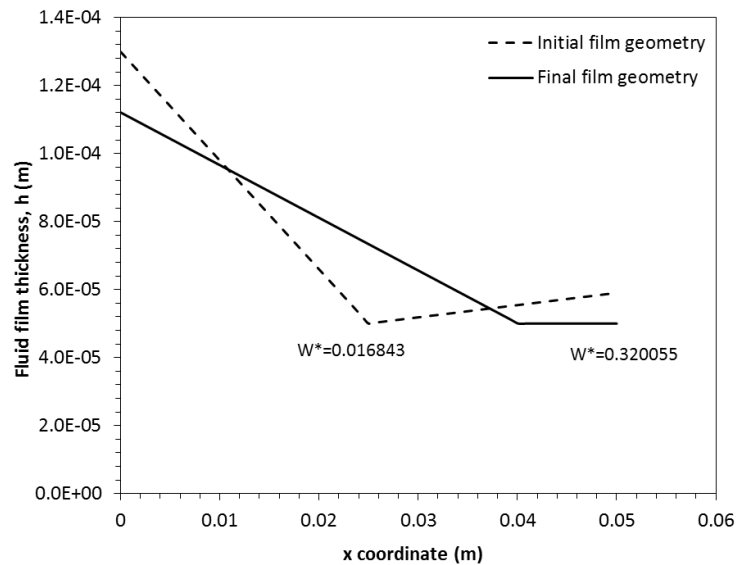


**Figure 23: Initial and optimal geometry of lubricant film geometry. Optimal values of the design variables are: $[h_1, h_2, l]$ = [0.000112, 0.00005, 0.040076].**

According to the three previous results, it is noted that independently from the initialization values of the design variables, in all the three optimization runs, the final result is the same, meaning that the point [h1, h2, l] = [0.000112, 0.00005, 0.04007] can be the global optimal.

## 4.4 Step – Maximum Load Capacity

In this section, the slider geometry under optimization is that presented in Figure 24, consisting of a step shape. Each region is described by a constant number, equal to the fluid film inlet height $h_1$ at point A and equal to minimum film thickness $h_0$ at point C up to D.
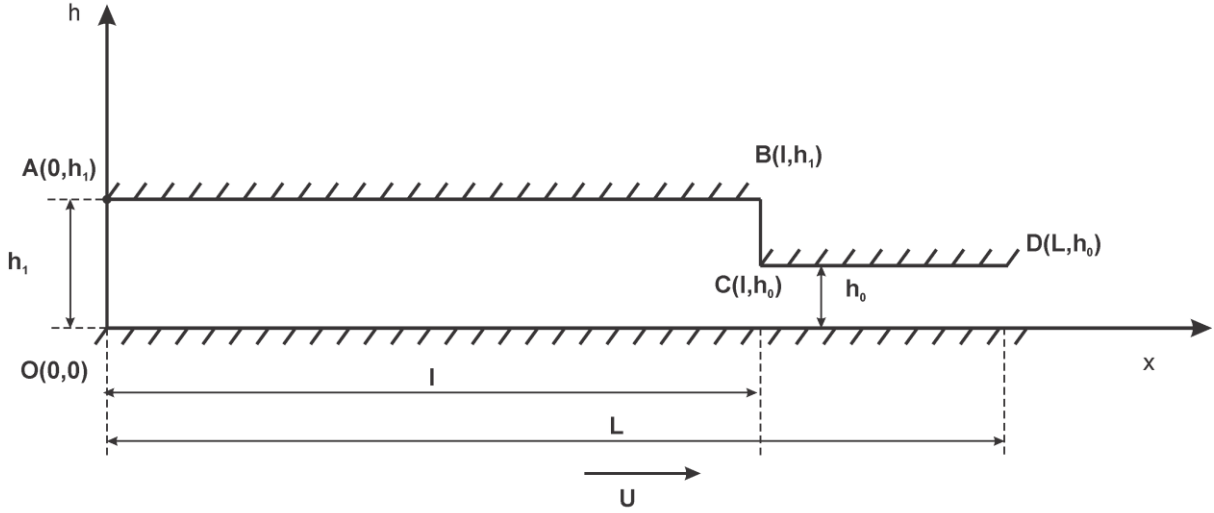


**Figure 24: Lubricated step-like slider.**

### 4.4.1 Primal Problem

The primal problem is governed by the Reynolds equation, as already seen in Eq. (37).

$$R = \frac{\partial^2 p}{\partial x^2} h^3 + 3h^2 \frac{\partial h}{\partial x} \frac{\partial p}{\partial x} - 6\mu U \frac{\partial h}{\partial x} = 0 \tag{74}$$

### 4.4.2 Adjoint Problem

The adjoint equation is also the same as the previous problem. The adjoint equation is:

$$\frac{d^2 \Psi}{dx^2} h^3 + 3h^2 \frac{dh}{dx} \frac{d\Psi}{dx} + 1 = 0 \tag{75}$$

where $\Psi$ is the adjoint variable

Similarly, the adjoint boundary conditions remain the same, namely:

$$\Psi(0) = 0$$
$$\Psi(L) = 0$$

### 4.4.3 Sensitivity Derivatives

$$\frac{\delta W}{\delta b} = 3\int_0^L \Psi \frac{d^2 p}{dx^2} h^2 \frac{\delta h}{\delta b} dx + 6\int_0^L \Psi \frac{dp}{dx} h \frac{\delta h}{\delta b} \frac{dh}{dx} dx +$$

$$3\int_0^L \Psi \frac{dp}{dx} h^2 \frac{\delta}{\delta b}\left(\frac{dh}{dx}\right) dx - 6\eta U \int_0^L \Psi \frac{\delta}{\delta b}\left(\frac{dh}{dx}\right) dx \tag{76}$$

In Eq. (76) the terms inside the integrals, except the $\delta/\delta b(.)$ terms, are replaced by the following symbols, for the purpose of simplicity:

$$Q_1 = 3\Psi \frac{d^2 p}{dx^2} h^2 + 6\Psi \frac{dp}{dx} h \frac{dh}{dx}$$

$$Q_2 = 3\Psi \frac{dp}{dx} h^2 - 6\mu U \Psi$$

So, Eq. (66) can be rewritten as follows:

$$\frac{\delta W}{\delta b} = \int_0^L Q_1 \frac{\delta h}{\delta b} dx + \int_0^L Q_2 \frac{\delta}{\delta b}\left(\frac{dh}{dx}\right) dx \tag{77}$$

At this point, the equations describing the step shape of Figure 24 should be found out. Line AB will be resulted knowing that the height of the inlet region is equal to $h_1$ and similarly line CD that the height of the outlet region is equal to the minimum film thickness $h_0$. Consequently:

Line AB: $h_{AB}(x) = h_1$

Line BC: $h_{BC}(x) = h_0$

The first try was based in the non-continuous form of the step function, which is the following one:

$$h(x) = \begin{cases} h_1, & x < l \\ h_0, & x \geq l \end{cases}$$

Using the above formulation stability problems were faced and the optimization process was unable to converge. So, similarly to the case of the two lines (converging-diverging), a sigmoidal function was used to simulate the step shape.

Despite this, the use of a sigmoidal function did not come without disadvantages. More specifically, the utilized sigmoidal function is the following one:

$$h(x,l) = \varphi \cdot h_1 + (1-\varphi) \cdot h_0 = \frac{1}{1+e^{m(x-l)}} h_1 + \left(1 - \frac{1}{1+e^{m(x-l)}}\right) h_0 \tag{78}$$

The factor $m$, decides how steep or smooth its curvature will be. High values of $m$ result in a shape very close to the real step function, while lower values lead to a smooth curve approximating the step shape.

Experimenting with the factor $m$, the following was observed; high values, meaning a shape closer to the real step, result in values of the adjoint sensitivity derivatives that don't match to the derivatives computed with the finite differences, while lower values of $m$, creating an approximate shape of the step, result in values of the adjoint sensitivity derivatives closer to the derivatives computed with the finite difference method. In addition to this, a decisive role in the matching of the two sensitivity derivatives has the number of discretization point, because more points are needed in order to model the steep geometry of the step. So, the grid points have been increased to 501, instead of 201 points that were used in all the previous cases. In Table 1, an example of the $m$ values, the corresponding shape and the sensitivity derivatives both of the adjoint and the finite difference method is presented.
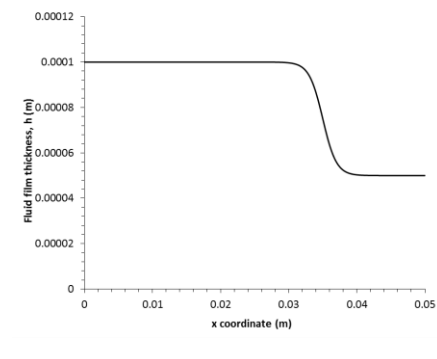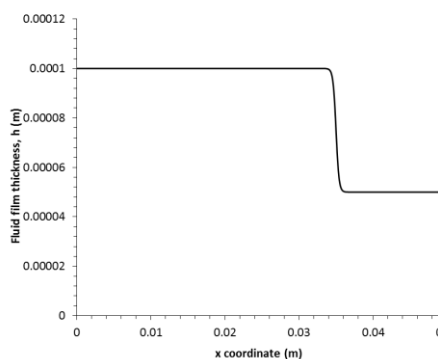
| | **m=1000** | m=5000 |
|---|---|---|
| Step shape |  |  |
| $\delta W/\delta h_1$ from adjoint | **-1.87E+08** | -2.70E+08 |
| $\delta W/\delta h_1$ from FD | **-1.86E+08** | -2.65E+08 |
| % difference of $\delta W/\delta h_1$ | **0.13%** | 1.98% |
| $\delta W/\delta l$ from adjoint | **-4.30E+04** | 1.11E+06 |
| $\delta W/\delta l$ from FD | **-5.26E+04** | 5.19E+05 |
| % difference of $\delta W/\delta l$ | **18.27%** | 114.08% |

**Table 1. Comparison of geometry and sensitivity derivatives for two different values of factor $m$ of Eq. (78).**

According to Table 1, the difference of 18.27% in the sensitivity derivative $\delta W/\delta l$ is considered to be acceptable. So the factor m is decided to be equal to _m=1000_, sacrificing a bit for the shape of the step geometry, but resulting in better match between the sensitivity derivatives computed with the adjoint method and finite differences methods.

The design variables for this problem are: $\vec{b} = [h_1, l]$.

According to Eq. (77) the derivatives $\dfrac{\delta h}{\delta \vec{b}} = \left[ \dfrac{\delta h}{\delta h_1}, \dfrac{\delta h}{\delta h_2}, \dfrac{\delta h}{\delta l} \right]$ and

$\dfrac{\delta}{\delta \vec{b}} \left( \dfrac{dh}{dx} \right) = \left[ \dfrac{\delta}{\delta h_1} \left( \dfrac{dh}{dx} \right), \dfrac{\delta}{\delta h_2} \left( \dfrac{dh}{dx} \right), \dfrac{\delta}{\delta l} \left( \dfrac{dh}{dx} \right) \right]$ should be calculated in order to find the

derivative $\dfrac{\delta W}{\delta b}$ at each optimization step.

➢ $\dfrac{\delta h}{\delta l} = \dfrac{\delta \varphi}{\delta l} h_1 + \varphi \cancelto{0}{\dfrac{\delta h_1}{\delta l}} + \cancelto{0}{\dfrac{\delta h_0}{\delta l}} - \dfrac{\delta \varphi}{\delta l} h_0 - \varphi \cancelto{0}{\dfrac{\delta h_0}{\delta l}} = \dfrac{\delta \varphi}{\delta l} (h_1 - h_0)$

  • $\dfrac{\delta \varphi}{\delta l} = \dfrac{m e^{m(x-l)}}{\left( 1 + e^{m(x-l)} \right)^2}$

➢ $\dfrac{\delta}{\delta l} \left( \dfrac{dh}{dx} \right) = \dfrac{d}{dx} \left( \dfrac{\delta h}{\delta l} \right) = \dfrac{d}{dx} \left( \dfrac{\delta \varphi}{\delta l} \right) (h_1 - h_0) + \dfrac{\delta \varphi}{\delta l} \dfrac{d}{dx} \cancelto{0}{(h_1 - h_0)} = \dfrac{d}{dx} \left( \dfrac{\delta \varphi}{\delta l} \right) (h_1 - h_0)$

  • $\dfrac{d}{dx} \left( \dfrac{\delta \varphi}{\delta l} \right) = \dfrac{m^2 e^{m(x-l)}}{\left( 1 + e^{m(x-l)} \right)^2} - \dfrac{2 m^2 e^{2m(x-l)}}{\left( 1 + e^{m(x-l)} \right)^3}$

➢ $\dfrac{\delta h}{\delta h_1} = \cancelto{0}{\dfrac{\delta \varphi}{\delta h_1}} + \varphi \dfrac{\delta h_1}{\delta h_1} + \cancelto{0}{\dfrac{\delta h_0}{\delta h_1}} - \cancelto{0}{\dfrac{\delta \varphi}{\delta h_1}} h_0 - \varphi \cancelto{0}{\dfrac{\delta h_0}{\delta h_1}} = \varphi$

  • $\dfrac{\delta}{\delta h_1} \left( \dfrac{dh}{dx} \right) = \dfrac{d}{dx} \left( \dfrac{\delta h}{\delta h_1} \right) = \dfrac{d\varphi}{dx} = -\dfrac{m e^{m(x-l)}}{\left( 1 + e^{m(x-l)} \right)^2}$

Finally, an external constraint is implemented upon the solution, setting the values of film thickness that are lower than the $h_{min}$, equal to it.

### 4.4.4 Results

Having computed the sensitivity derivative of W, using Eq. (77), the optimization loop can be initiated, as already presented in Figure 14. Several runs have been performed, with three different initialization points, almost equally distributed within the fluid film region, as follows:

1. $h_1 = 100$ μm, $l = 0.035$



**Figure 25: Non-dimensional load capacity trend along the optimization loop, $W^*_{opt}=0.03423$.**

The initial geometry and the optimal geometry after the optimization procedure are presented in Figure 26.



**Figure 26: Initial and optimal geometry of lubricant film geometry. Optimal values of the design variables are: $[h_1, l] = [0.000093, 0.034055]$.**

2. $h_1 = 80 \ \mu m$, $l = 0.015$
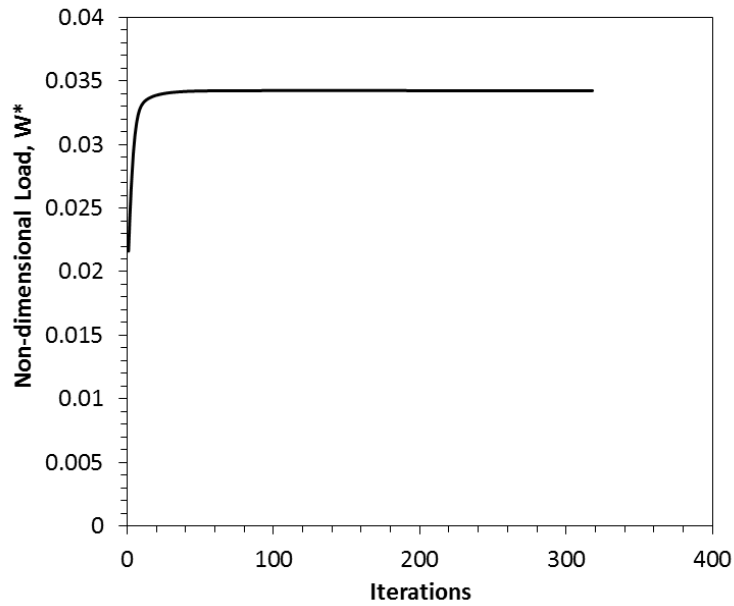


**Figure 27: Non-dimensional load capacity trend along the optimization loop, $W^*_{opt}$=0.03423.**

The initial geometry and the optimal geometry after the optimization procedure are presented in Figure 28.



**Figure 28: Initial and optimal geometry of lubricant film geometry. Optimal values of the design variables are: [$h_1$, l] = [0.000093, 0.034055].**
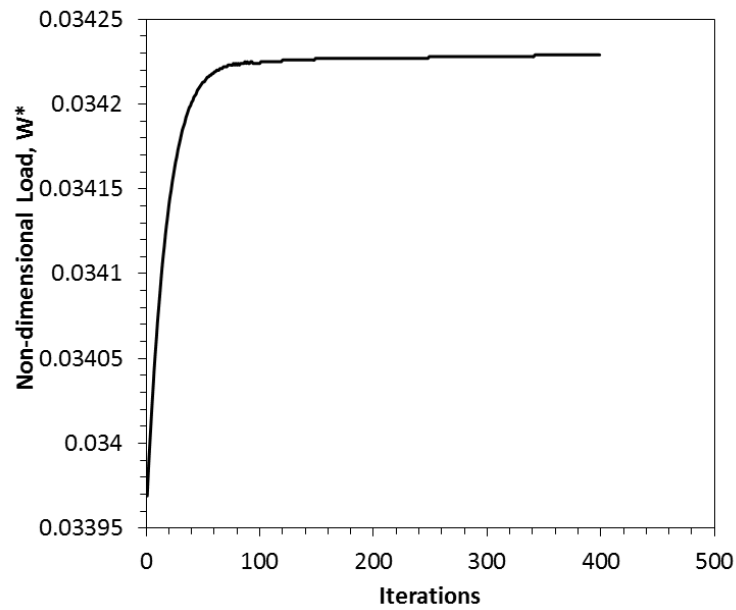
3. $h_1 = 130$ μm, $l = 0.025$
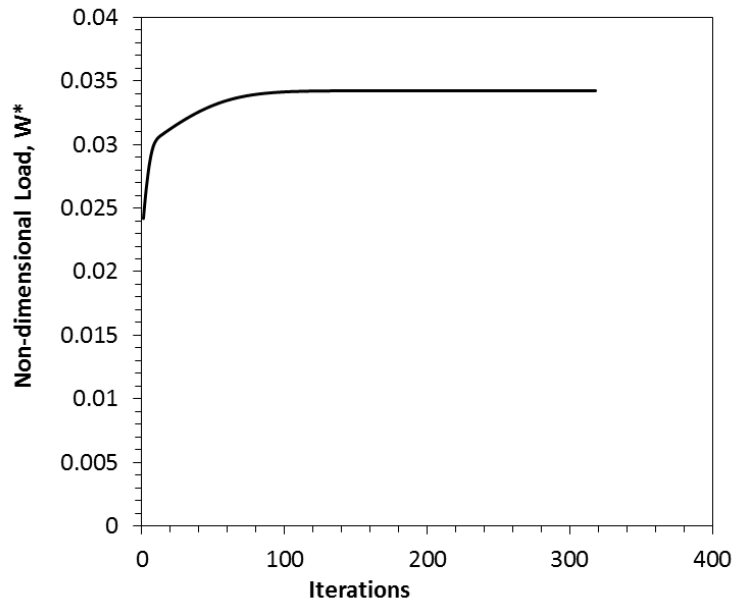


**Figure 29: Non-dimensional load capacity evolution along the optimization loop, $W^*_{opt}$=0.03423.**

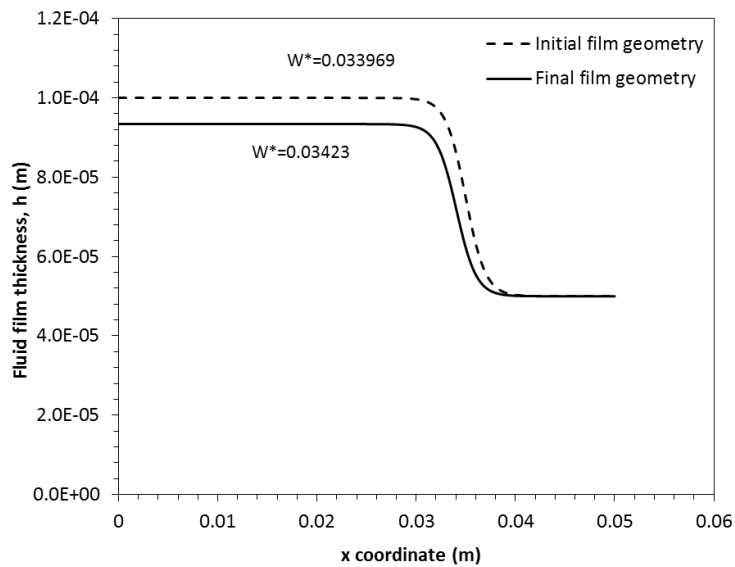The initial geometry and the optimal geometry after the optimization procedure are presented in Figure 30.



**Figure 30: Initial and optimal geometry of lubricant film geometry. Optimal values of the design variables are:  [$h_1$, l] = [0.000093, 0.034055].**

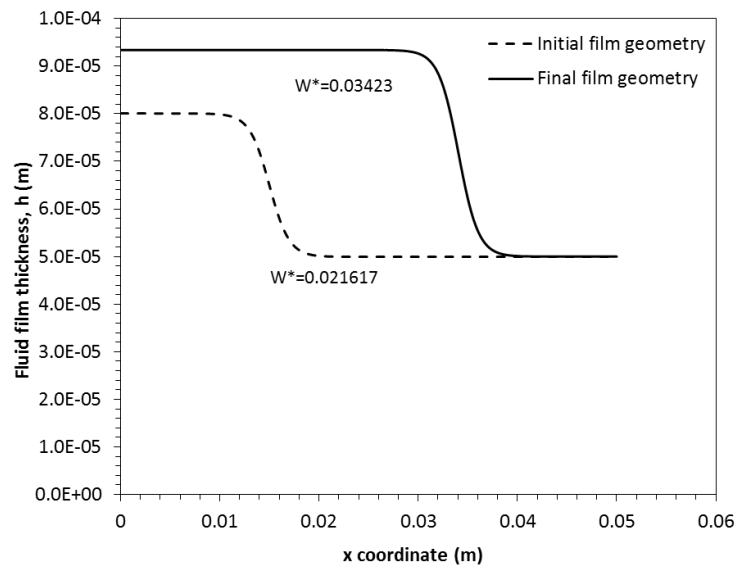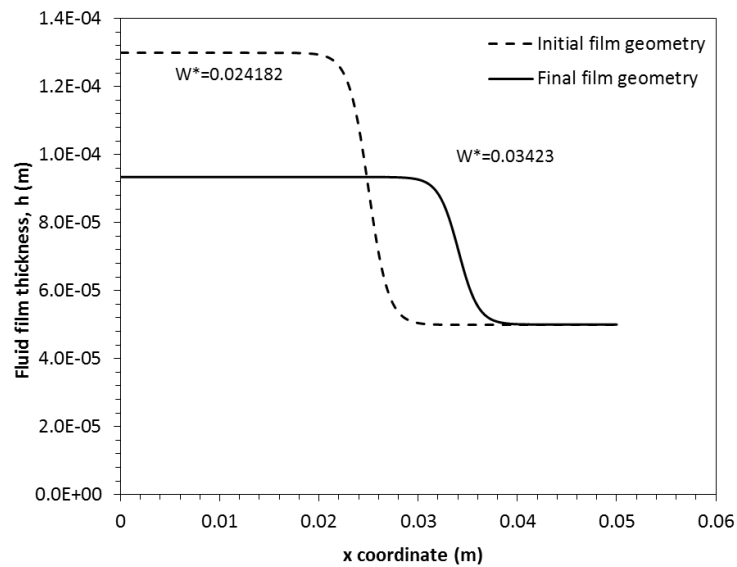According to the three previous results, it is noted that independently from the initialization values of the design variables, in all the three optimization runs, the final result is the same, meaning that the point [h1, h2, l] = [0.000093, 0.034055] can be the global optimal.

## 4.5 Nodal Parameterization

In this section, a second method is used to parameterize the converging slider. The initial geometry is defined for each case and, then, the nodal values of film thickness, $h_i$, are considered as the design variables. In this way, the geometry is completely free to self-adjust to the optimal shape for each different case, always depending on the initial shape.

This means that if the solution domain is discretized in N points, then the number of design variables is N and, at each optimization cycle, N derivatives $\delta W/\delta h_i$ must be computed. The values of these derivatives reflect how much the load capacity W changes if each point undergoes an infinitesimal offset around its position.

These derivatives provide information about what regions of the surface should be displaced and in what direction, in order to improve the performance. When the derivatives are plotted upon the geometry, the resulting figure is the so-called sensitivity map of the surface which is a valuable help to the designer.

In other cases, being also the case of the present study, these derivatives can be used in a conjugate gradient method to proceed to a better geometry, leading after some optimization steps to the optimal one.

Until now, in tribology and hydrodynamic lubrication surfaces, stochastic optimization methods, using a confined number of design variables, have been used to conclude to optimal geometries, such as the simple converging slider [7]. An adjoint method with the nodal values of the geometry being the design variables, can lead to a completely different shape, because the geometry is described from the discrete values of film thickness providing a great potential of diversity, see Figure 31.
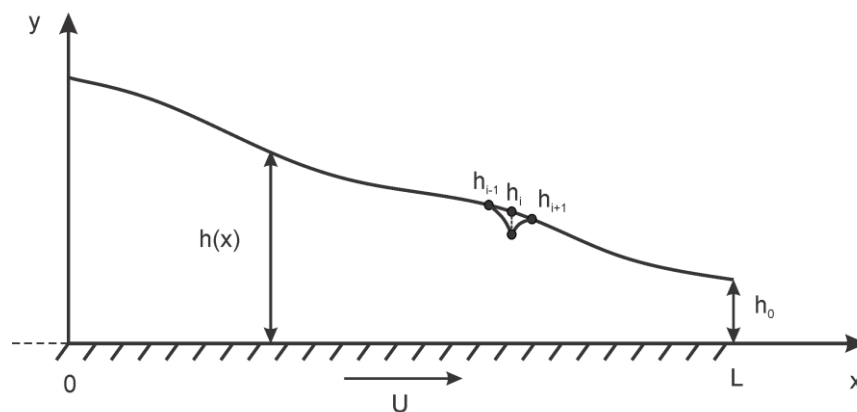


**Figure 31: Slider with an example of sensitivity derivative calculation [1].**

In Figure 31, an example of the way of computating the sensitivity derivative $\dfrac{\delta W}{\delta h_i}$ is presented. This derivative expresses how much the objective function, here the load carrying capacity, changes when the point $h_i$ is slightly moved, almost as much as the epsilon value, in the one or the other direction.

The optimization process, along with the adjoint equation and the adjoint boundary conditions are the same to that described in Chapter 4. The only change in this problem is the

geometry expression, which now consists of the nodal values of the film thickness, meaning that the number of design variables is equal to the discretization points along the x-axis. So, the following are repeated only for reasons of completeness:

### 4.4.1 Primal Problem

The primal problem is governed by the Reynolds equation, as already seen in Eq. (37).

$$R = \frac{\partial^2 p}{\partial x^2} h^3 + 3h^2 \frac{\partial h}{\partial x} \frac{\partial p}{\partial x} - 6\mu U \frac{\partial h}{\partial x} = 0 \tag{79}$$

It is solved using the finite difference method and an iterative solver for the pressure, p. Dirichlet boundary conditions are applied at both ends of the solution domain.

### 4.4.2 Adjoint equation

The adjoint equation is also the same as the previous problem, where the only design variable was only the divergence ratio k, because the adjoint equation has been derived generally for a vector of design variables b. The adjoint equation is:

$$\frac{d^2\Psi}{dx^2} h^3 + 3h^2 \frac{dh}{dx} \frac{d\Psi}{dx} + 1 = 0 \tag{80}$$

where $\Psi$ is the adjoint variable

Similarly, the adjoint boundary conditions remain the same, namely:

$$\Psi(0) = 0$$
$$\Psi(L) = 0$$

### 4.4.3 Nodal Sensitivity Derivatives

This is where the main change, between parameterizing the geometry with one (or more) parameters and expressing it with the nodal value of film thickness, is located. The derivatives of the objective functions are now calculated with respect of the local film thickness of each node, and their number is equal to the number of the discretization points.

The generalized formula defining the derivative of the objective function W with respect to any design variables vector b has already been presented in Eq. (48) and is repeated below:

$$\frac{\delta W}{\delta b} = 3\int_0^L \Psi \frac{d^2 p}{dx^2} h^2 \frac{\delta h}{\delta b} dx + 6\int_0^L \Psi \frac{dp}{dx} h \frac{\delta h}{\delta b} \frac{dh}{dx} dx +$$

$$3\int_0^L \Psi \frac{dp}{dx} h^2 \frac{\delta}{\delta b}\left(\frac{dh}{dx}\right) dx - 6\mu U \int_0^L \Psi \frac{\delta}{\delta b}\left(\frac{dh}{dx}\right) dx \qquad (81)$$

For the current case, vector $\vec{b}$ consists of all the h(i) values along the x-axis:

$$\vec{b} = \left[ h_1, h_2, ..., h_i, ... h_{N-1}, h_N, \right]$$

So Eq. (81) now can be written as follows:

$$\frac{\delta W}{\delta h_k} = \int_0^L \underbrace{3\Psi \frac{d^2 p}{dx^2} h^2}_{A} \frac{\delta h}{\delta h_k} dx + \int_0^L \underbrace{6\Psi \frac{dp}{dx} h \frac{dh}{dx}}_{B} \frac{\delta h}{\delta h_k} dx +$$

$$\int_0^L \underbrace{3\Psi \frac{dp}{dx} h^2}_{C} \frac{\delta}{\delta h_k}\left(\frac{dh}{dx}\right) dx + \int_0^L \underbrace{\left(-6\mu U\right) \Psi}_{D} \frac{\delta}{\delta h_k}\left(\frac{dh}{dx}\right) dx \qquad (82)$$

The various terms in the above equation must be written as sums from i=0 to i=N, because of the terms $\frac{\delta h}{\delta h_k}$ and $\frac{\delta}{\delta h_k}\left(\frac{dh}{dx}\right)$, which become active only at node i=k. Consequently $\frac{\delta h}{\delta h_k}$ can be replaced by the Kronecker delta, while the term $\frac{\delta}{\delta h_k}\left(\frac{dh}{dx}\right)$ demands a more careful analysis, because it expresses how sensitive the spatial derivative of geometry is to the local shift of node $h_k$.

In Eq. (82), the terms within the integrals, apart from the sensitivity derivatives of $h_k$, are denoted by the following block letters, for brevity,

$$A_i = \Psi_i \frac{d^2 p}{dx^2}\bigg|_i h_i^2 \qquad (83)$$

$$B_i = 6\Psi_i \frac{dp}{dx}\bigg|_i h_i \frac{dh}{dx}\bigg|_i \qquad (84)$$

$$C_i = 3\Psi_i \frac{dp}{dx}\bigg|_i h_i^2 \qquad (85)$$

$$D_i = -6\eta U \Psi_i \qquad (86)$$

So, Eq. (82) is now rewritten as:

$$\frac{\delta W}{\delta h_k} = \int_0^L A \frac{\delta h}{\delta h_k} dx + \int_0^L B \frac{\delta h}{\delta h_k} dx + \int_0^L C \frac{\delta}{\delta h_k}\left(\frac{dh}{dx}\right) dx + \int_0^L D \frac{\delta}{\delta h_k}\left(\frac{dh}{dx}\right) dx =$$
$$\int_0^L (A+B) \frac{\delta h}{\delta h_k} dx + \int_0^L (C+D) \frac{\delta}{\delta h_k}\left(\frac{dh}{dx}\right) dx$$
(87)

In Eq. (87) the two terms will also be distinguished and elaborated separately. These two integrals are also substituted with two variables to make easier the following analysis.

$$\frac{\delta W'}{\delta h_k} = \int_0^L (A+B) \frac{\delta h}{\delta h_k} dx$$

$$\frac{\delta W''}{\delta h_k} = \int_0^L (C+D) \frac{\delta}{\delta h_k}\left(\frac{dh}{dx}\right) dx$$

δW'/δh_k term

For the integral of these terms of Eq. (87) the trapezoidal rule will be used and the general expression for the derivative of one point is the following one:

$$\frac{\delta W'}{\delta h_k} = \frac{\Delta x}{2}(A_1 + B_1)\delta_{1k} + \sum_{i=2}^{N-1}(A_i + B_i)\delta_{ik} + \frac{\Delta x}{2}(A_N + B_N)\delta_{Nk}$$
(88)

Kronecker Delta is equal to unity only when i=k, so the derivative of the first, last and all the rest nodes are equal to:

$$\frac{\delta W'}{\delta h_1} = \frac{\Delta x}{2}(A_1 + B_1)$$
(89)

$$\frac{\delta W'}{\delta h_k} = \Delta x(A_k + B_k)$$
(90)

$$\frac{\delta W'}{\delta h_N} = \frac{\Delta x}{2}(A_N + B_N)$$
(91)

δW''/δh_k term

These refer to the terms of Eq. (87) that include the sensitivity derivative of the first spatial derivative of film thickness and are equal to:

$$\frac{\delta W''}{\delta h_k} = \int_0^L (C+D) \frac{\delta}{\delta h_k}\left(\frac{dh}{dx}\right) dx$$
(92)

In the standard adjoint problems these terms are generally difficult to cope with, because they represent how sensitive the spatial derivative of the design variable is, when the design variable changes.

At this point, the following problem arose. When the dh/dx terms is discretized using central differences, dh/dx becomes completely insensitive to the changes in the central point $h_i$, because the first derivative depends on the variable values at points i+1 and i-1.

So, second order backward differences were used for almost the whole domain, because the value of the central node exists in the formula. The first four nodes demand forward differences.

At first, the finite difference formula of dh/dx for an internal point is written using backwards differences:

$$\left.\frac{dh}{dx}\right|_{i=(3,N]} = \frac{3h_i - 4h_{i-1} + h_{i-2}}{2\Delta x}$$

And for the first two points, this is written obligatorily with forward differences, despite the fact that these terms will remain inactive during the following analysis.

$$\left.\frac{dh}{dx}\right|_{i=1,2} = \frac{-h_{i+2} + 4h_{i+1} - 3h_i}{2\Delta x}$$

The integral of Eq. (92), using the trapezoidal rule to approximate it, for a random internal node, can be expanded as:

$$\frac{\delta W''}{\delta h_k} = \frac{\Delta x}{2}(C_1 + D_1)\frac{\delta}{\delta h_k}\left(\left.\frac{dh}{dx}\right|_1\right) + \sum_{i=2}^{N-1}(C_i + D_i)\frac{\delta}{\delta h_k}\left(\left.\frac{dh}{dx}\right|_i\right) + \frac{\Delta x}{2}(C_N + D_N)\frac{\delta}{\delta h_k}\left(\left.\frac{dh}{dx}\right|_N\right)$$

$$\frac{\Delta x}{2}(C_1 + D_1)\frac{\delta}{\delta h_k}\left(\frac{-h_3 + 4h_2 - 3h_1}{2\Delta x}\right) + \Delta x(C_2 + D_2)\frac{\delta}{\delta h_k}\left(\frac{-h_4 + 4h_3 - 3h_2}{2\Delta x}\right) + ... + \tag{93}$$

$$\Delta x(C_i + D_i)\frac{\delta}{\delta h_k}\left(\frac{3h_i - 4h_{i-1} + h_{i-2}}{2\Delta x}\right) + ... + \frac{\Delta x}{2}(C_N + D_N)\left(\frac{3h_N - 4h_{N-1} + h_{N-2}}{2\Delta x}\right)$$

Because of the fact that forward differences have been used for the first 2 nodes and backwards for the rest of the domain, several terms are repeated within the sums, leading to inaccurate calculation of the derivative at these points and the two neighboring ones. So, the assumption has been made that the derivative $\delta W''/\delta h_k$ of the first four points is equal to the derivative of the fifth one. More specifically, substituting the node for which the derivative is calculated into Eq. (93), the following expressions result:

$$\frac{\delta W"}{\delta h_5} = \Delta x \left( C_5 + D_5 \right) \frac{\delta}{\delta h_5} \left( \frac{3h_5 - 4h_4 + h_3}{2\Delta x} \right) + \Delta x \left( C_6 + D_6 \right) \frac{\delta}{\delta h_5} \left( \frac{3h_6 - 4h_5 + h_4}{2\Delta x} \right) +$$

$$\Delta x \left( C_7 + D_7 \right) \frac{\delta}{\delta h_5} \left( \frac{3h_7 - 4h_6 + h_5}{2\Delta x} \right) = \Delta x \left( C_5 + D_5 \right) \left( \frac{3}{2\Delta x} \right) + \Delta x \left( C_6 + D_6 \right) \left( -\frac{2}{\Delta x} \right) + \qquad (94)$$

$$\Delta x \left( C_7 + D_7 \right) \left( \frac{1}{2\Delta x} \right) = \frac{3}{2} \left( C_5 + D_5 \right) - 2 \left( C_6 + D_6 \right) + \frac{1}{2} \left( C_7 + D_7 \right)$$

As already mentioned, the derivative of the first four points is set equal to the derivative of fifth point, given by Eq. (94). So:

$$\frac{\delta W"}{\delta h_{k=[1,4]}} = \frac{\delta W"}{\delta h_5} = \frac{3}{2} \left( C_5 + D_5 \right) - 2 \left( C_6 + D_6 \right) + \frac{1}{2} \left( C_7 + D_7 \right) \qquad (95)$$

Thinking in the similar way as in Eq. (94), the derivatives are calculated for the following points too:

$$\frac{\delta W"}{\delta h_{k=[5,N-3]}} = \frac{3}{2} \left( C_k + D_k \right) - 2 \left( C_{k+1} + D_{k+1} \right) + \frac{1}{2} \left( C_{k+2} + D_{k+2} \right) \qquad (96)$$

$$\frac{\delta W"}{\delta h_{N-2}} = \frac{1}{2} \left( C_{N-2} + D_{N-2} \right) - \frac{1}{2} \left( C_{N-1} + D_{N-1} \right) + \frac{1}{4} \left( C_N + D_N \right) \qquad (97)$$

$$\frac{\delta W"}{\delta h_{N-1}} = \frac{3}{2} \left( C_{N-1} + D_{N-1} \right) - \left( C_N + D_N \right) \qquad (98)$$

$$\frac{\delta W"}{\delta h_N} = \frac{3}{4} \left( C_N + D_N \right) \qquad (99)$$

Finally, in order to present the final formula of the sensitivity derivative of each node, the terms of Eq. (89)-(91) and Eq. (96)-(99) must be merged, yielding the final expressions:

$$\frac{\delta W}{\delta h_1} = \frac{\Delta x}{2} \left( A_1 + B_1 \right) + \frac{\delta W"}{\delta h_5} = \frac{\Delta x}{2} \left( A_1 + B_1 \right) + \frac{3}{2} \left( C_5 + D_5 \right) - 2 \left( C_6 + D_6 \right) + \frac{1}{2} \left( C_7 + D_7 \right) \qquad (100)$$

$$\frac{\delta W}{\delta h_{k=[2,5]}} = \Delta x \left( A_k + B_k \right) + \frac{\delta W"}{\delta h_5} = \Delta x \left( A_k + B_k \right) + \frac{3}{2} \left( C_5 + D_5 \right) - 2 \left( C_6 + D_6 \right) + \frac{1}{2} \left( C_7 + D_7 \right) \qquad (101)$$

$$\frac{\delta W}{\delta h_{k=[6,N-3]}} = \Delta x \left( A_k + B_k \right) + \frac{3}{2} \left( C_k + D_k \right) - 2 \left( C_{k+1} + D_{k+1} \right) + \frac{1}{2} \left( C_{k+2} + D_{k+2} \right) \qquad (102)$$

$$\frac{\delta W}{\delta h_{N-2}} = \Delta x \left( A_k + B_k \right) + \frac{1}{2} \left( C_{N-2} + D_{N-2} \right) - \frac{1}{2} \left( C_{N-1} + D_{N-1} \right) + \frac{1}{4} \left( C_N + D_N \right) \tag{103}$$

$$\frac{\delta W}{\delta h_{N-1}} = \Delta x \left( A_k + B_k \right) + \frac{3}{2} \left( C_{N-1} + D_{N-1} \right) - \left( C_N + D_N \right) \tag{104}$$

$$\frac{\delta W}{\delta h_N} = \frac{\Delta x}{2} \left( A_N + B_N \right) + \frac{3}{4} \left( C_N + D_N \right) \tag{105}$$

### 4.4.4 Optimization loop

In this case, the optimization procedure follows the next steps, see also Figure 14 in flow-chart form for a single design variable though.

1. Initialization of the design variables vector. In this case, these are the nodal values of film thickness, $h_i$, meaning that the number of design variables is equal to the grid size of the problem.
2. Solution of the primal problem, i.e. of Eq. (79), providing the pressure distribution along the solution domain.
3. Calculation of the objective function, here the load carrying capacity of the slider, Eq. (43), by integrating the pressure field along the x direction. This value can also be non-dimensionalized by Eq. (52), in order to compare cases with different sizes.
4. Solution of the adjoint problem, Eq. (80), providing the values of the Lagrange multiplier $\Psi$ along the solution domain.
5. Calculation of the sensitivity derivatives $\dfrac{\delta W}{\delta \vec{h}}$ , utilizing Eq. (100) - (105). The variables A, B, C and D appearing in these equation are given by Eq. (83) - (86) and are functions of pressure and Lagrangian $\Psi$, that have already been computed in steps 2 and 4 respectively.
6. Computation of the new film thickness, using the conjugate gradient method, as follows:

$$\vec{h}_{new} = \vec{h}_{old} + s \frac{\delta W}{\delta \vec{h}} \Leftrightarrow \begin{bmatrix} h_1^{new} \\ \vdots \\ h_i^{new} \\ \vdots \\ h_N^{new} \end{bmatrix} = \begin{bmatrix} h_1^{old} \\ \vdots \\ h_i^{old} \\ \vdots \\ h_N^{old} \end{bmatrix} + s \begin{bmatrix} \dfrac{\delta W}{\delta h_1} \\ \vdots \\ \dfrac{\delta W}{\delta h_i} \\ \vdots \\ \dfrac{\delta W}{\delta h_N} \end{bmatrix}$$

The value of $s$ is always carefully selected in order to adjust to the units of the current problem. If W is in measured in Newton and $h$ in micrometers then $s$ should be around

$10^{-15}$-$10^{-16}$. An external constraint is also implemented upon the solution, setting the values of film thickness that are lower than the $h_{min}$, equal to it.

7.  After updating the geometry ($h$), the procedure starts again from step 2, and is repeated many times, until the derivatives converge to zero.

### 4.4.5 Validation

When solving an optimization problem such as the current one it is of utmost importance to validate the values of the sensitivity derivatives computed by the adjoint method, against the corresponding derivatives calculated from a finite differences scheme.

According to the finite difference scheme, at each point of the solution domain, the design variable, here the local film thickness, is moved upwards and downwards from the initial position, by a distance equal to $\delta h$=0.01 μm. After each displacement, the new value of the objective function, here the load carrying capacity, is computed and, finally, the sensitivity derivatives are derived by:

$$\frac{\delta W}{\delta h_i} = \frac{W_{+\delta h} - W_{-\delta h}}{(h_i + \delta h) - (h_i - \delta h)} = \frac{W_{+\delta h} - W_{-\delta h}}{2\delta h} \tag{106}$$

where:

$W_{+e}$ is the load capacity after the point $h_i$ has been shifted from its initial position +e upwards.

$W_{-e}$ is the load capacity after the point $h_i$ has been shifted from its initial position -e downwards.

So, in Figure 32 a comparison is presented between the $\frac{\delta W}{\delta h_i}$ cmputed from the adjoint method and the $\frac{\delta W}{\delta h_i}$ computed from finite differences, as seen in Eq. (106). These derivatives are computed starting from a simple converging slider geometry, with a converging ratio equal to 1.2.
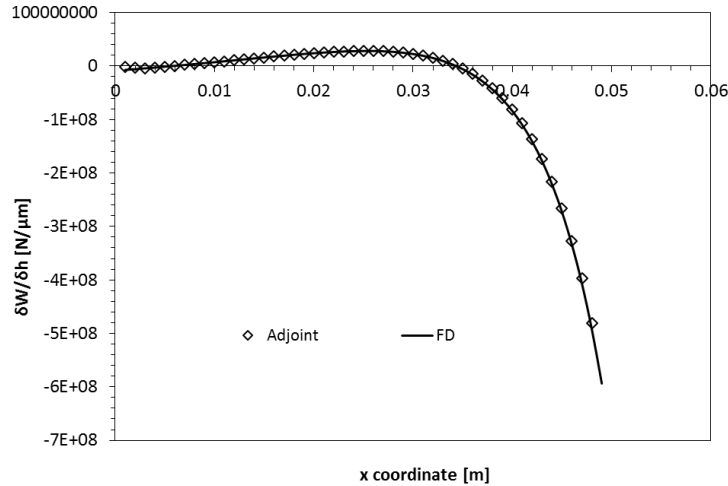
**Figure 32: Comparison of δW/δh between the adjoint and the finite difference method.**

A very good match can be observed between the two methods, meaning that the adjoint method developed in this chapter, calculates correctly the sensitivity derivatives.

### 4.4.6 Results

It is of high importance here to remind that our target is the maximization of load carrying capacity. This optimization problem is solved for a constant minimum film thickness, $h_{min}$. If $h_{min}$ is not constrained, the problem has a trivial solution equal to a value very close to zero, because, while the cross section is reduced, the developed pressure increases.

Consequently, in order to constraint the minimum film thickness, the following procedure has been implemented. Starting from the initial film thickness profile, the minimum value of the film thickness is computed. Afterwards, during the optimization loop, if any resulted value of film thickness is below the threshold value of $h_{min}$, this is set equal to $h_{min}$.

It must also be clarified that this method is a deterministic one and there is no guarantee that will necessarily find the global optimum. The resulted geometry of each run is different and heavily depends on the initial shape given to the geometry, during the initialization step.

The initial geometries that has been tested is the plain convergent slider, with a variety of converging ratios.

Three different cases of the plain converging slider were tested, varying the converging ratio of the slider from 0.1 up to 5. It is reminded that the design variables are the nodal values of the film thickness and not the converging ratio. The trend of the non-dimensional capacity for each cases is presented in the following figures, along with the point after which the solution starts to present instabilities and the iterations are terminated. Additionally, the initial

68

geometry and the geometry corresponding to the terminal point are also shown in the following figures.

1. Initial point: k=0.1

In Figure 33 the trend of the non-dimensional load capacity against the optimization iterations (a) and the initial and final geometry (b) are presented.
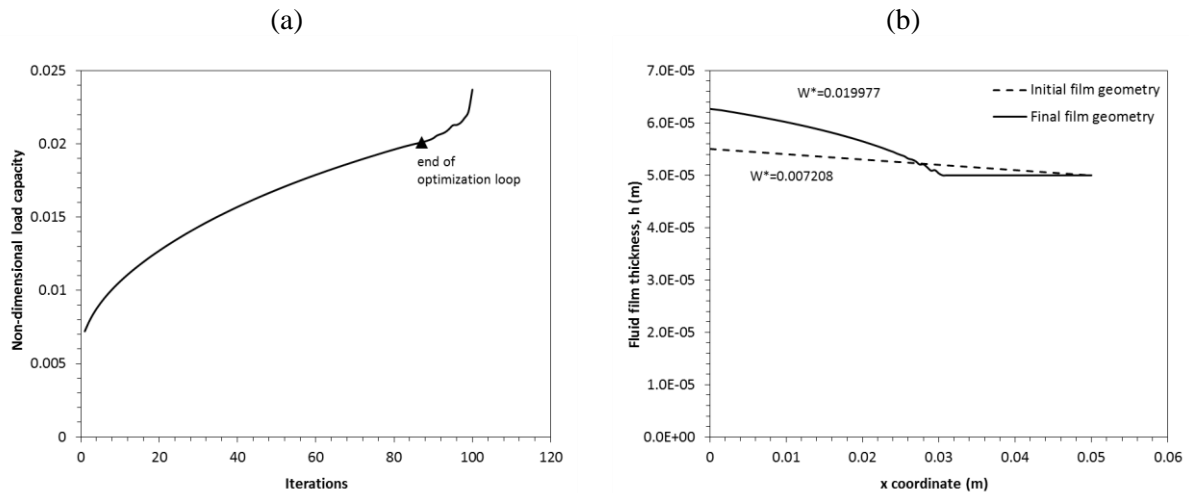
Figure 33: Results for initial converging ratio k=0.1: (a) non-dimensional load capacity against iterations, final optimization step is marked with triangle (b) initial and final (triangle) film thickness profile.

2. Initial point: k=1.2

It must be noted that the geometry corresponding to converging ratio k=1.2 is the optimal solution that resulted from the adjoint optimization of chapter 4.1, where the design variable was only the converging ratio $k$. Here, the interesting point is to find out if there is an even better solution, when the design variables are the nodal values of the film thickness. In Figure 34, the trend of the non-dimensional load capacity against the optimization iterations (a) and the initial and final geometry (b) are presented.

(a)                                                                                    (b)



**Figure 34: Results for initial converging ratio k=1.2: (a) non-dimensional load capacity against iterations, final optimization step is marked with triangle (b) initial and final (triangle) film thickness profile.**

3. Initial point: k=5

In Figure 35, the trend of the non-dimensional load capacity against the optimization iterations (a) and the initial and final geometry (b) are presented.
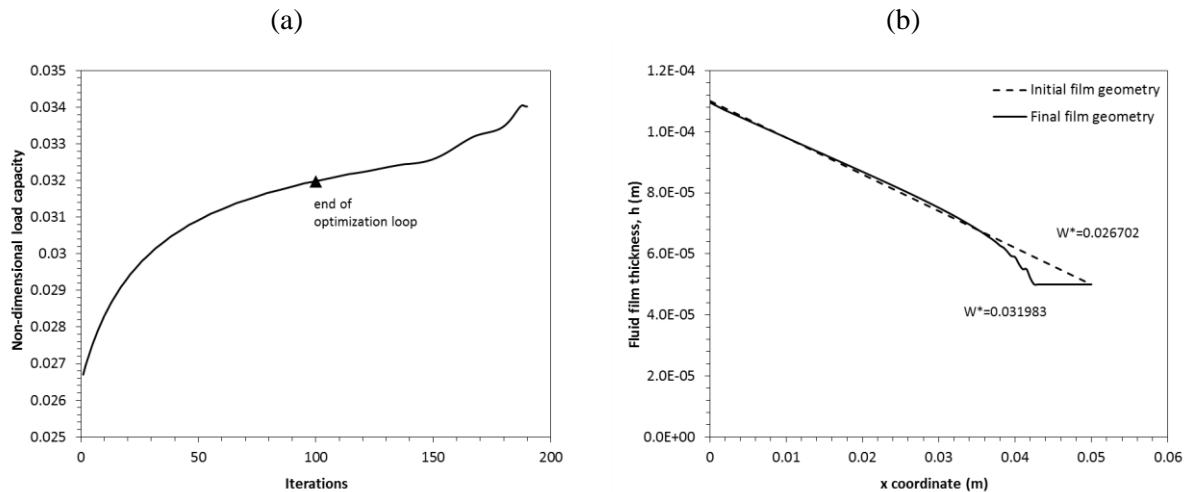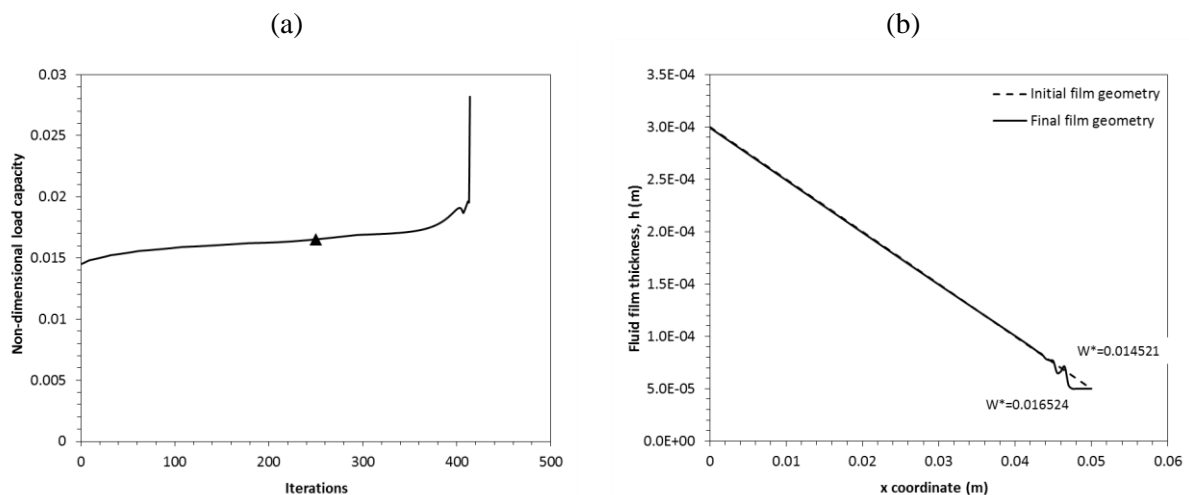
(a)                                                                                    (b)



**Figure 35: Results for initial converging ratio k=5: (a) non-dimensional load capacity against iterations, final optimization step is marked with triangle (b) initial and final (triangle) film thickness profile.**

Observing the results presented above, the first obvious remark is that in all the cases after some point the solution starts to present instabilities. This happens due to the fact that the derivatives are computed with finite differences and so after some point they start to take very high values even close to infinite. Second, it is obvious that the film thickness geometry is less affected as the converging ratio $k$ increases. This can be explained as the steeper the geometry the less the effect of the slider geometry upon the values of the objective function, meaning that the load capacity is rather insensitive to the changes of the film thickness profile.

70

# 6. Conclusions and future work

In the framework of this thesis, the continuous adjoint optimization method has been developed in order to optimize the design of certain geometries of tribological contacts. The mathematical formulation has been performed for each geometry separately and the sensitivity derivatives have been thoroughly elaborated, as their accuracy may affect the final result of the optimization. More specifically, in order to verify our results, for each case the values of the sensitivity derivatives computed from the adjoint method are compared to the ones computed from the finite difference method and a good match was found in all the cases.

Subsequently, a MATLAB code was developed, in order to run the optimization, computing at each step the sensitivity derivatives and proceeding to the next step with a steepest desent method. For each case, the process has been initiated from different points in order to secure that the method has reached a global optimal point and not a local one. This was achieved in all the cases except the last one where the design variables are the nodal values of film thickness, because instability problems occurred. For that reason, in the latter case, the loop was terminated before oscillations of the solution start.

Concluding, the adjoint method is a very useful tool for the optimization of hydrodynamic lubrication systems as it indicates the areas that have greater effect on the objective function and towards what direction they should be moved in order to improve it. It is also a very useful computational tool for the sensitivity derivatives of a certain geometry, as the computational cost is almost equal to cost of the primal problem.

The suggested subject for future research is the case where the design variables are the nodal values of the film thickness, and especially the numerical instability of the solution. For instance, the computed sensitivity derivatives could be filtered with a polynomial method, in order to smoothen out the peaks it exhibits. Another suggestion is to use Bezier curves to describe the geometry, reducing the points controlling the fluid film shape, probably making the optimization smoother, but reducing the degrees of freedom of the geometry.

# 5. Literature

1. Holmberg K., Erdemir A., "Friction and Energy Saving", 50th Anniversary Celebration of the Jost Report, Institution of Mechanical Engineers, London, UK, 2.3.2016.
2. Volund A., Klit P., "Measurement and Calculation of Frictional Loss in Large Two-Stroke Engines", Copenhagen, T.E.U., 2003.
3. Clausen N.B., "Marine Diesel Engines-How Efficient can a Two Stroke Engine be?", http://www.ship-efficiency.org/onTEAM/pdf/Clausen.pdf, 10.02.2014.
4. Antoniou A., Wu-Sheng L., "Practical Optimization – Algorithms and Engineering Applications", Springer, 2007
5. Giannakoglou K. C., "Methods of Deterministic and Stochastic Optimization and Applications", Notes of MSc Lesson, Athens 2012.
6. Stachowiak G., Batchelor A., "Engineering Tribology", Butterworth Heinemann, 2011.
7. Papadopoulos C.I., Efstathiou E.E., Nikolakopoulos P.G., Kaiktsis L., "Geometry Optimization of Textured Three-Dimensional Micro-Thrust Bearings", ASME Journal of Tribology, vol. 133, 041702, pp. 1-14, 2011.
8. Pavlioglou S.K. et al, "Tribological Optimization of Thrust Bearings Operated with Lubricants of Spatially Varying Viscosity", ASME GT2014-25292, pp 1-10, 2014.
9. Dobrica M.B., Fillon M., Pascovici M.D., Cicone T., "Optimizing Surface texture for hydrodynamic lubricated contacts using mass-conserving numerical approach", Proc. IMechE Vol. 224 Part J: J. Engineering Tribology, 2010
10. Anderson P., Tamminen J., Sandström C. E., "Piston ring tribology - A literature survey", VTT Industrial Systems.
11. Khonsari M.M., Booser E.R., "Applied Tribology: Bearing Design and Lubrication", Chichester: John Wiley & Sons Ltd, p. 201, pp. 215-216, pp. 225-227, 2008.
12. Raptis L., "Software development for the solution of hydrodynamic lubrication problems in main bearings of marine Diesel engines", Diploma Thesis, Athens, March 2014.
13. US Department of Energy, "DOE Fundamentals Handbook - Mechanical Science, Vol. 1 of 2, Diesel Engine Fundamentals", Washington 1993